Published in final edited form as:
J Mol Biol. 2007 May 25; 369(1): 108–128. doi:10.1016/j.jmb.2007.01.091.

Crystal Structure of Tryptophanyl-tRNA Synthetase Complexed with Adenosine-5′ Tetraphosphate: Evidence for Distributed Use of Catalytic Binding Energy in Amino Acid Activation by Class I Aminoacyl-tRNA Synthetases

Pascal Retailleau[1], **Violetta Weinreb**[2], **Mei Hu**[3], and **Charles W. Carter Jr.**[2,¶]

[1] Service de Cristallochimie, ICSN-CNRS, Gif/Yvette, 91198 Fr

[2] Department of Biochemistry and Biophysics, University of North Carolina, Chapel Hill, North Carolina 27599-7360

[3] Department of Microbiology, Duke University, Durham, NC. 27

Abstract

Tryptophanyl-tRNA synthetase (TrpRS) is a functionally dimeric ligase, which specifically couples hydrolysis of ATP to AMP and pyrophosphate to the formation of an ester bond between tryptophan and the cognate tRNA. TrpRS from *Bacillus stearothermophilus* binds the ATP analogue, adenosine-5′ tetraphosphate, AQP, competitively with ATP during pyrophosphate exchange. Estimates of binding affinity from this competitive inhibition and from isothermal titration calorimetry show that AQP binds 200 times more tightly than ATP both under conditions of induced-fit, where binding is coupled to an unfavourable conformational change, and under exchange conditions, where there is no conformational change. These binding data provide an indirect experimental measurement of +3.0 kcal/mole for the conformational free energy change associated with induced-fit assembly of the active site. Thermodynamic parameters derived from the calorimetry reveal very modest enthalpic changes, consistent with binding driven largely by a favorable entropy change. The 2.5 Å structure of the TrpRS:AQP complex, determined *de novo* by X-ray crystallography, resembles that of the previously described, pre-transition state TrpRS:ATP complexes. The anticodon-binding domain untwists relative to the Rossmann-fold domain by 20% of the way toward the orientation observed for the Products complex. An unexpected tetraphosphate conformation allows the $\tilde{\gamma}$ and $\tilde{\delta}$ phosphate groups to occupy positions equivalent to those occupied by the $\tilde{\beta}$ and $\tilde{\gamma}$ phosphates of ATP. The β-phosphate effects a 1.11 Å extension that relocates the α-phosphate toward the tryptophan carboxylate while the PPi mimic moves deeper into the KMSKS loop. This configuration improves interactions between enzyme and nucleotide significantly and uniformly in the adenosine and PPi binding subsites. A new hydrogen bond forms between S194 from the class I KMSKS signature sequence and the PPi mimic. These complementary thermodynamic and structural data are all consistent with the conclusion that the tetraphosphate mimics a transition-state in which the KMSKS loop develops increasingly tight bonds to the PPi leaving group, weakening linkage to the Pα as it is relocated by an energetically favourable domain movement. Consistent with extensive mutational data on Tyrosyl-tRNA synthetase, this aspect of

¶Corresponding author: Department of Biochemistry and Biophysics, CB 7260, University of North Carolina at Chapel Hill, Chapel Hill, NC 27599-7260, Tel: (919) 966-3263, FAX: (919) 966-2852, Email: E-mail: carter@med.unc.edu.

the mechanism develops high transition-state affinity for the adenosine and pyrophosphate moieties, which move significantly, relative to one another, during the catalytic step.

Keywords

Induced-fit; mechanistic enzymology; phosphoryl-transfer; catalytic use of binding energy; class I aminoacyl-tRNA synthetases

Introduction

Because of its widespread use in biosynthetic, biomechanical, and regulatory processes, nucleophilic substitution at phosphoryl groups is among the most studied bimolecular reactions in biology [1]. Uncatalyzed rates of phosphoryl-solvolysis are quite slow, in the range of 10^{-5}/min, and bimolecular reactions such as amino acid activation are slower, about 10^{-8}/Mole/min [2]. Metal ions (Mg^{++}) accelerate these rates by only perhaps three-fold [1; 3].

Understanding the relative roles of general acid or base catalysis, emerging charge stabilization, mechanical distortion, and other catalytic effects in enzyme mechanisms that accelerate this reaction $10^{10} – 10^{14}$ fold requires characterization of the transition state in relation to the ground state(s). Phosphoryl transfer is usually described with reference to two extreme transition-state configurations: a fully *dissociative*, SN_1-like mechanism and a fully *associative*, SN_2-like mechanism (Figure 1; see [1; 4; 5; 6] for reviews). These extremes are distinguished by the extent to which the nucleophile and leaving group participate in bond-making and bond-breaking. In transition states with dissociative character, the bond to the leaving group is weakened or broken first, while in those with associative character, the approach of the nucleophile is strengthened before the bond to the leaving group weakens.

Participation of both bond-making and bond-breaking processes leads in general to a continuous, two-dimensional surface [5]. This surface is characterized by approximately equal barrier heights along many different possible trajectories, any of which might be stabilized by a variety of different interactions with enzymatic active sites [6], making it difficult to assess which path is taken by a particular enzyme.

The amino acid activation step catalyzed by class I aminoacyl-tRNA synthetases (aaRS), in which the leaving group is inorganic pyrophosphate instead of phosphate, deserves renewed attention in this context. The amino acid activation mechanism has been extensively studied by site-directed mutagenesis and pre-steady state kinetics [7; 8; 9; 10], and by crystallographic methods [9; 11; 12; 13; 14; 15; 16; 17; 18; 19; 20; 21]. However, despite these efforts, mechanistic descriptions have been limited to modelling in-line displacement of the PPi leaving group by the α-carboxylate of the amino acid without identifying specific interactions that develop in the transition-state complexes.

Most enzymes that catalyze phosphoryl transfer and which have been characterized structurally, exhibit significant potential transition-state complementarity to a pentavalent phosphate group, consistent with associative character. In contrast, the Class I *B. stearothermophilus* tryptophanyl-tRNA synthetase (TrpRS) structural reaction profile [11; 12; 13; 15] suggests a different transition state with dissociative character. First, active site residues do not appear to provide specific interactions capable of differentiating between ground-state and transition-state configurations of the α-phosphate. Second, those catalytic residues identified by mutation of the closely related TyrRS active site interact either with the ribose or the pyrophosphate moieties [8]. Finally, TrpRS catalysis is associated with a large domain rearrangement between the Pre-transition state (PreTS) and Products structures, in which the

pyrophosphate binding site formed by the KMSKS loop relocates by ~1.6 Å. The relative absence of interactions to the α-phosphate, the abundance of distributed catalytic interactions to the adenosine and pyrophosphate moieties, and the implication that the TrpRS transition state occurs during dynamic domain movement consistently point to a novel mechanism to stabilize the phosphoryl-transfer transition state involved in amino acid activation by TrpRS, TyrRS, and perhaps class I aaRS in general.

One effective way to characterize enzymatic transition states structurally is to mimic them with stable compounds, or transition-state analog inhibitors [22]. Transition state mimics are a mixed blessing. On the one hand, it is impossible in principal to imitate precisely in a stable analog the geometry and electron distributions of a transition state which, by definition is the least stable, and hence shortest-lived species along a reaction path [23]. For this reason all such analogs mimic only a subset of the features of the actual transition state. The descriptive phrase, transition-state analog, therefore evokes a variety of interpretations, and examples of compounds designated as transition-state mimics approach the transition state more or less adequately.

On the other hand, such inhibitors can provide useful, approximate structural models. When they can be crystallized with the enzymes they inhibit, interactions that strengthen in the transition state complex and possibly accelerate the reaction rate can be identified. Thus, such analogs provide a valuable link between structure and function.

The validity of inferences drawn from structural analogs of transition states depends on several criteria expected for such complexes [22; 24]. First, the compounds themselves should capture stably some distinctive aspect – geometry, charge distribution, polarity - of the altered substrate configuration in the transition state. Second, their affinities should substantially exceed those for the substrates they mimic. Third, to attribute the increased affinity to transition-state-like features, enzyme:transition-state-analog complex structures should reveal strengthening of interactions already present in the binding of substrates, together with new interactions evoked by those parts of the analogs that mimic changes in the transition state. Fourth, it is also reasonable that the active site will intensify the physical enclosure of the analog and limit the access of solvent, relative to what is observed for substrates. Finally, experimental variables that alter the enzymatic rate acceleration should have parallel effects on the analog binding affinity.

We describe here experiments with the ATP analogue, adenosine tetraphosphate, AQP. The affinity and crystal structure of a TrpRS:AQP complex appear to meet each of the first four criteria. Moreover, protein engineering experiments to identify a minimal, functionally active TrpRS catalytic domain suggest an important experimental test along the lines of the fifth criterion. These data provide a novel and coherent structural representation of the distributed interactions by which class Ic enzymes use binding energy for catalysis, first outlined experimentally by Fersht and co-workers [7; 8] who showed that catalytically relevant interactions occur throughout the surface of the nucleotide [7; 8].

Results

AQP binding affinity

Competitive inhibition—AQP is not a substrate; it does not support incorporation of ^{32}P-pyrophosphate into adenine nucleotide (we did not test for its ability to generate acylated $tRNA^{Trp}$). It is an inhibitor, competitive with ATP. The inhibition constant, measured by steady-state kinetics, is 2.0 mM.

Although K_i is a true thermodynamic dissociation constant, several considerations condition its interpretation. AQP, like ATP, has a high affinity for Mg^{++}, which is present in excess under the assay conditions. Yet, as described below, the bound form of AQP does not contain Mg^{++}. Nor are there any water molecules near the ligand that might represent this ion. The binding equilibrium leading to inhibition is therefore coupled to an equilibrium in solution between AQP and Mg^{++}•AQP that heavily favours the complexed form, so that the concentration of the uncomplexed AQP is very much smaller than K_i (see, for example, [ref 25]). Put another way, the TrpRS-AQP interaction is strong enough to compete with the AQP-Mg^{++} interaction. Thus, as the K_i is based on the total AQP concentration in the assay rather than that of the uncomplexed form, a correct estimate for the affinity, K_i*, requires estimating the concentration of free AQP in the assay from the dissociation constant for the Mg^{++}•AQP complex in solution:

$$Mg^{++} \bullet AQP \overset{K_D}{\rightleftarrows} AQP + Mg^{++}$$
$$AQP + TrpRS \overset{K_I^*}{\rightleftarrows} TrpRS \bullet AQP \qquad (I)$$

We estimate the Mg^{++}•AQP dissociation constant following [26] to be, ~2.18×10^{-6} M[1]. Under this assumption, the actual concentration of uncomplexed AQP at half-saturation is ~ 2.2 μM.

Isothermal titration calorimetry—Titrations of two TrpRS concentrations (6 μM and 60 μM) were carried out with AQP in the absence of Mg^{++}. Data were fitted to a sequential binding model with two different kinds of binding sites [27] as described in Methods (Figure 2a). Calorimetric determinations were noisy, owing to the small enthalpy changes and the limiting amount of AQP we had synthesized. Use of two different protein concentrations sharply constrained the combinations of binding affinity and binding enthalpy parameters (Table 1) that would fit both curves simultaneously, reducing their uncertainty to less than five percent. Dissociation constants for the two successive AQP molecules are 18 μM and 40 μM, respectively.

Comparison of the three AQP binding processes reflected in K_I* and the ITC titrations is complicated by the fact that binding can induce conformational changes with non-negligible intrinsic free energies [11; 28]. There are three, distinct binding scenarios, indicated by the schematic logos in Figure 2b. These include: (i) binding to the Open conformation (blue) and (ii) rebinding into the assembled active site vacated by a ligand (exchange; green), neither of which involve conformational changes, and (iii) binding of a second ligand to the open, singly-liganded dimer (induced-fit; blue=>green), which confounds the nucleotide-binding affinity with the conformational change. In light of these three scenarios, the AQP binding affinities in Figure 2a are consistent with other, related thermodynamic measurements, including the AQP inhibition constant and the affinities of TrpRS for ATP [11], Figure 2b. In particular, AQP affinity is stronger by 200-fold both in exchange and in induced-fit binding processes, which have been determined for both nucleotides.

As the enthalpy changes associated with successive binding events are rather small, ± ~ 1 Kcal/mole, AQP binding is largely entropy driven (Table 1). This result is consistent with the large reduction in the entropy of water molecules that results from dissolution of

[1]These calculations make several assumptions, extrapolating conservatively from the values given by Adolfson and Moudrianakis (1978) for the intrinsic affinity of Mg for ADP (12000) and ATP (140000) and the mu values (1.5 and 3.1, respectively, to values of 800000 and 3.8, respectively. These two values are highly correlated. So, this extrapolation is subject to revision by experimental data we cannot provide without synthesizing more AQP.

polyphosphates into water [29]. The binding affinity for both adenine nucleotides therefore likely results from replacing water molecules bound to the phosphate groups with protein side chains. The structural results also suggest that the differential binding affinity for AQP, relative to ATP, arises largely from an increase in the number and strength of such hydrogen-bonded interactions and the release of water molecules bound to the TrpRS•ATP complex in the case of AQP.

The conformational free energy change associated with induced-fit

The thermodynamic data from Figure 2 are sufficient to allow an experimental determination of the free energy change for the conformational equilibrium between Open and Closed, PreTS states in the presence and absence of ligands, using the thermodynamic cycle in Figure 3. The latter value is equivalent to the allosteric constant [24]. The cycle in Figure 3 resolves the free energies associated with the induced-fit active-site assembly into purely conformational and purely ligand binding equilibria, which implicitly include any proton transfers associated with binding (we have not measured the pH dependence of either ATP or AQP affinity). We assume in addition from the crystallographic symmetry of the Closed, PreTS state that dissociation constants for both nucleotide-binding events to that form are identical.

Successive dissociations from the fully liganded Open state are distinct; experimental determination of the first is convolved with the free energy change associated with the induced-fit assembly in the doubly liganded form. The determinations of comparable equilibrium constants for both ATP and AQP, however, allow us to de-convolve the ligand binding and conformational free energies of this process by regression analysis (Table 2), which is motivated by the near exact differences between the two ligands in the induced-fit and exchange binding scenarios.

The regression model is:

$$\Delta G = \langle \Delta G_{Q,T} \rangle + \Delta G_{QvsT} * \mathrm{Lig} + \Delta G_{\text{induced-fit}} * \mathrm{IF} \quad (2)$$

where the dependent variable, ΔG, is the observed free energy obtained from each equilibrium constant in Table 2, Lig is either 0 or 1 depending on whether the ligand is ATP or AQP, and IF is 0 or 1 depending on whether or not the process involves a conformational change. The three adjustable parameters are $\langle \Delta G_{Q,T} \rangle$, the average free energy for binding either T or Q to either state, ΔG_{QvsT}, the incremental free energy for binding Q, relative to T, and $\Delta G_{\text{induced-fit}}$, the conformational free energy for reversing the induced-fit closure of the fully liganded, open dimer. The model accounts for the four measured equilibrium constants associated with the cycle with $R^2 = 0.999$ and an F-ratio probability of 0.007. The $\Delta G_{\text{induced-fit}}$ value, together with the dissociation constants, provide estimates for the free energies of top and side equilibria of the thermodynamic cycle in Figure 3. The right-hand side equilibrium free energies are given by the exchange dissociation constants. The bottom branch is the allosteric constant describing the conformational equilibrium in the absence of adenine nucleotides and can be calculated by completing the cycle. Allosteric constants for the two nucleotides, +3.08 (for T) and +3.00 (for Q) are in excellent agreement, placing an upper limit on the error in the simplifying assumptions.

Structure of TrpRS crystallized with AQP

A binary crystalline complex was obtained by co-crystallization of TrpRS with AQP. The crystallizing solution buffered at pH 7.5 was made up with sodium citrate and Mg^{++}, in addition to the cyclohexylammonium counter ion accompanying AQP. The crystal grew in the tetragonal $P4_32_12$ space group with unit cell dimensions close to those of the pre-transition

state (PreTS) crystalline complexes with ATP (1M83) and ATP plus tryptophanamide (1MAU), also grown in citrate (a = b = 62.18 Å c = 220.88 Å *vs* a = b = 62.13 Å c = 217.81Å suggesting the closed, PreTS TrpRS conformation as defined previously [11]. The slight non-isomorphism of the 1.3% increase along the c axis is consistent with conformational changes described below with respect to PreTS state ATP complexes. The polypeptide chain runs from the N-terminal (Met 1) to the C-terminal (Arg 328) through the electron density map defined by unbiased experimental phases. As the asymmetric unit contains a single monomer, crystal packing imposes symmetry on the functionally asymmetric dimer. Nevertheless, for low-energy hydrogen-bonding interactions to form between the two, symmetry-related Gln94 side-chains across the molecular dyad they must assume alternate, complementary configurations in each monomer, breaking the crystallographic symmetry.

Isotropic B-values, $<B_{CA}>$ = 46.5, are substantially elevated in this complex relative to those in the two PreTS crystals $<B_{CA}>$ = 30.23 (1MUA), 20.41 (1M83). Consistent with elevated B-values, (Figure 4) density is poorly defined for a certain number of side chains (Asp28, Arg104, Glu116, Lys178, Arg182, Lys191, Lys211, Glu225, Lys233, Arg259, Arg327 & 328). These sites are either accessible to solvent and/or belong to loops (loop 112-119 in the RF is expected to anchor the CCA acceptor stem and loop comprising residues 220 -235 and 259 - 266 in the SD to bind the anticodon) that recognize the cognate tRNA. The refined model consists of 2,613 protein atoms in accordance with the monomer sequence. A bound AQP nearly coincident with the location of Mg^{++}•ATP in 1M83 and 1MAU was modelled and subsequently refined into difference density in the nucleotide-binding cavity (Figure 4).

TrpRS conformation—The TrpRS monomer consists of two domains, a Rossmann dinucleotide binding fold of ~200 residues (RF), which starts with the N-terminal beta strand A, and a smaller domain of ~90 residues that includes a four-helix bundle, the C-terminal helix of which extends back by ~35 residues with a pronounced kink, past the RF, where it interacts across the dimer interface. Binding sites for tryptophan and ATP are created opposite each crossover connection in the RF. The highly twisted β-sheet brings three peptide signatures, TIGN on the helix αA, GxDQ on helix αE, and KMSKS together to bind the nucleotide, helix αD providing specificity-determining elements for amino acid binding whose configurations remain essentially unchanged in the course of catalysis.

From comparisons between several TrpRS structures [11; 12; 13; 15], it appeared that the functional TrpRS domain boundary actually falls between the TIGN and KMSKS signatures, on one hand, and the GxDQ signature with the main body of RF, on the other hand. Coordinated movements between the two domains can be resolved into two internal coordinates, reflecting the hinge opening between domains and their relative twist [28]. The hinge motion is effected via rotation of the axis of helix αA, relative to the rest of the RF. Its motion is tightly coupled to that of the 4-helix bundle via the hydrophobic side chains of I16 and M193, from TIGN and KMSKS respectively, together with I20, which join a substantial hydrophobic core within the four helix bundle containing the anticodon-binding site to form what we have called the small domain (SD). The rigid-body motions of the SD provide an important link between active-site chemistry and the orientation of the anticodon-binding site. The twist involves internal rotations within the interface between helix αA and the SD, for which the largest displacement resides in the KMSKS loop.

The overall conformation of TrpRS in complex with AQP is quite similar to that from the pre-transition state complex with ATP, obtained under identical crystallizing conditions [11]. Formation of this conformation implies that AQP provides binding energy comparable to that for ATP, apparently necessary and sufficient to trigger both the 7.5° hinge-closing and 9° twisting rotations of the SD [28] relative to the RF, closing the active site around the nucleotide to form the closed, PreTS state and restraining access to the tryptophan binding pocket.

Structural differences between the AQP complex and those reported previously for the PreTS conformations, 1MAU and 1M83, are subtle (Figure 5a). Naïve superposition of the AQP complex and the PreTS complexes yields RMSD values of 0.707 Å (1M83) and 0.746 Å (1MAU), while the two PreTS complexes agree with an RMSD of 0.384 Å. The two previously described PreTS structures afford the opportunity to test the significance of these differences. For this purpose, the Rossmann folds of all structures were superimposed as described at the end of the experimental section, and then the r.m.s coordinate differences were determined between the Cα atoms of all aligned structures and separately for the domains.

The main contribution to the RMSDs between PreTS and AQP complexes comes from a reorientation of the SD, which untwists toward the Products conformation, Figure 5a. This shift, albeit small (the r.m.s. coordinate difference over the RF excluding the loop 111-119 is less than 0.3 and that over the SD is more than 0.7), places the SD in between positions assumed in the PreTS states and in the adenylate Products complex (Figure 5b). Multiple regression models indicate that both replacing ATP by AQP and the SD orientation (twist angle) are significant contributors of the RMSD values, with t-test probabilities of 2×10^{-4}, and 3×10^{-3}, respectively.

Untwisting of the SD in the Products conformation displaces the KMSKS sequence and the leaving PPi group by 1.42 Å from its position in the ATP complex [11]. The twist angles of the PreTS, AQP, and Products complexes are 8.9°, 8.1°, and 4.6°. The AQP structure therefore places the KMSKS loop approximately 20% (0.19) of the way toward the Products conformation, consistent with a similar estimate based on RMSDs (0.16). We return to the possible dynamic participation of domain orientation in the catalytic process in the discussion.

A last, conspicuous difference between the two binary, closed complexes lies in the path of the loop (112-119) that forms a gate over the active site and probably helps anchor the tRNA's 3′ terminus for aminoacylation. The terminal residues (112-113) of the α-helix (106-113) in the PreTS state unwind, creating a significantly modified path for the main chain in this region. The effect is to move this loop in the opposite direction from the KMSKS loop across the active site, thereby slightly opening the crevice to the active site.

Absence of Magnesium and effective binding affinity of AQP—The electron density for the nucleotide-binding site is shown in Figure 4 and modelling of an AQP molecule into Fourier difference maps is unambiguous. Pα and Pγ show up in the density at the level of sulphur atoms whereas Pβ and Pδ are at a level equivalent to the most stable backbone carbons. Curiously, no density appears for a counter cation in the AQP complex. Polyphosphates have high affinity for magnesium ions in solution, and Mg^{++} ion was present in excess in crystallization. However, the position of the β-phosphate replaces much of the volume occupied by magnesium in the ATP complexes, and no density appears elsewhere near the phosphates. As noted above, there appears, to be a competition between Mg^{++}:AQP and AQP:TrpRS interactions, such that AQP binds to TrpRS at least as tightly as it does to Mg^{++}.

AQP configuration and environment—The adenosine moiety superimposes remarkably precisely on the position taken in the ATP complex (Figure 6), making in most cases essentially the same interactions with the protein. Carbonyl oxygen atoms from Ile183 and Met193 recognize the N6 amino group, and the purine ring is centered on the carbonyl-carbon of the conserved Gly21 as in all TrpRS•adenine nucleotide complexes [11; 15].

If the RF domains are aligned (Figure 6a), the adenosine, ribose, and terminal pyrophosphate moieties of ATP and AQP superimpose closely. The ribose position has also changed little from its position in the ATP closed complex, and therefore differs from its unique position observed in the ATP- indolmycin complex [30]. However, Gly144 from the $_{14}$4GxDQ$_{147}$

sequence which faces the ribose, has shifted toward the O2′ hydroxyl allowing the nitrogen group to make an H-bond with OD_2 of Asp146 (Table 3).

Three water molecules found in all TrpRS crystal structures that contain the adenosine moiety (five PreTS complexes and six Products complexes) are also preserved in the immediate neighborhood of the nucleotide in the AQP complex (Figure 6b). One (W557) stacks over the purine ring bridging the D146 carboxylate to the C-terminal β-strand of the Rossmann fold (residue 181). Another (W541) lies between the ribose 3′-OH group and the S6 hydroxyl group and the G7 carbonyl oxygen. S6 is structurally homologous to C35 in *B. stearothermphilus* TyrRS, which plays a significant role in transition stabilization, probably via a homologous bound water molecule [31]. The third, W513, links the T15 hydroxyl group of the TIGN signature to the non-bridging O2β,γ of the nucleotide. This water molecule may protonate the transition state configuration of that oxygen, assuming a role played by histidine in the canonical HIGH signature. Three additional water molecules (gray) observed in the ATP complexes are missing from the AQP complex.

More unexpected was the accommodation of a longer phosphate tail by the TrpRS active site. Thermodynamic linkage between binding free energies and conformations implies that different enzyme conformations selectively bind different ligands. By this reasoning, the α, β, and γ phosphates of AQP might be expected to superimpose on the ATP triphosphate, with its terminal phosphate extending beyond the exit gate of the active site, delimited by side chains of Ser196 and Lys111. However, rather than extending fully, the AQP terminal pyrophosphate moiety occupies very nearly the same position as the pyrophosphate leaving group in the ATP complexes, “scrunching” the β-phosphate in between it and the AMP moiety.

Major differences between the two adenine nucleotide ligands are thus confined to the configuration of the Pα phosphate and Mg^{++} ion in the ATP complexes and the Pα and Pβ phosphate groups of AQP. Fitting the Pγ and Pδ phosphates into the pocket formed by the KMSKS loop compels the polyphosphate to turn sharply at the β-phosphate, which therefore overlaps the volume occupied by the Mg^{++} ion in PreTS complex structures. The extra phosphate relocates the α-phosphate by ~0.4 Å toward the tryptophan carboxylate nucleophile while pressing the PPi mimic deeper into the KMSKS loop. As a consequence, the bridging oxygen atom between Pβ and Pγ (O3β) assumes a position 2.73 Å from Pα, compared to the corresponding distance in ATP (1.62 Å; Figure 6a). This arrangement is quite close to that expected for a dissociative transition state.

The presence of the additional β-phosphate group imposes two unusual interactions on nearby electronegative groups: Oδ1_146-O2β and O1β – O1δ (bottom two rows in Table 3). The distances of these contacts, 2.41 Å, implies that they must share protons to minimize electrostatic repulsion. Both interactions therefore entail an increase of several pH units in the pKas of the respective constituent acidic groups. Their contributions to binding affinity therefore are likely to be unfavourable [32]. The Pβ oxygen atoms also form weak hydrogen bonds to $N\varepsilon_2$-Gln147 and $N\varepsilon_2$-Gln9. The former interaction is absent entirely, while the latter is directed toward the α-phosphate (3.08 Å) and Mg^{++} (3.8 Å) in the PreTS ATP complexes. Thus, the β-phosphate seems to exploit an environment similar to that of the Mg^{++} ion whose volume it replaces.

Comparison of binding interactions in the ATP and AQP complexes—The subtle repositioning of the PPi mimic significantly improves its interactions with the KMSKS and loop (Figure 6c). Notably, a hydrogen bond between S194 and K192 in the ATP complexes is broken in the AQP complex, and both residues make hydrogen bonds to phosphate oxygen atoms, one of which (S194-O3δ) is new. The novelty of the S194 interaction motivated us to inventory all contacts between TrpRS and both adenine nucleotides.

The resulting inventory, with standard deviations based on the two PreTS crystal structures, 1M83 and 1MAU, is compiled according to binding group subsite in Table 3. All subsites show shortened contacts with the AQP ligand, relative to ATP. These changes amount to 7 standard deviations in the pyrophosphate-binding subsite, to 5 standard deviations in the ribose-binding subsite, and to 9 standard deviations in the adenine-binding subsite. The only contact that does not shorten is that between the 3′OH group and W541. The differential contacts include both van der Waals and hydrogen-bonding interactions. They are uniform and widely distributed throughout the entire volume occupied by adenine nucleotide. Notably, the least dramatic changes, both in quantity and in significance occur in the environment of the α-phosphate, which shorten by less than one standard deviation. Thus, the strengthened interactions to the adenosine and PPi moieties, together with the three displaced water molecules (Figure 6a) provide the only convincing structural basis for the higher affinity of the TrpRS:AQP complex.

Discussion

The mechanisms by which Class Ic aaRS catalyze amino acid activation have been the object of considerable investigation. Mutational studies of TyrRS combined with pre-steady-state kinetics [8; 33] demonstrated catalytic roles for numerous residues remote from the site of chemical changes in the transition state for tyrosine activation. Although lacking in many structural details, these studies sketched convincingly the outlines of a novel source of catalytic rate enhancement. Participation of these residues is both significant and transient; they affect only the nucleotide; and, in the case of the PPi-binding subsite, they are limited to a role in transition-state binding. Despite these data, the overall mechanism remains sketchy. While they are crucial, mutational and kinetic data can be interpreted in different ways, because they lack important structural details. Thus, they are hard to match with models of the transition state configuration of ATP itself during the catalyzed in-line displacement of PPi by the α-carboxylate. The structure of the TrpRS:AQP complex brings complementary new structural data to bear on how the remote residues implicated by Fersht's studies might contribute to the mechanism.

We suggest in this discussion how data reported here bear on six questions relevant to the catalytic mechanisms of amino acid activation by aaRS: (1) Why is AQP unable to function as a substrate? (2) What is the catalytic role of the single Mg^{++} ion in the rate acceleration observed for class I aaRS? (3) How does the metal interact with other potential sources for electrostatic catalysis? (4) Are AQP:protein interactions similar to any of those responsible for accelerating amino acid activation? (5) Does domain motion (untwisting) play a catalytic role, and if so, how? (6) Do class I and class II aaRS share a common transition state stabilization mechanism?

Why is AQP not a substrate?

Chemically, triphosphate should be approximately as good a leaving group as pyrophosphate. If the TrpRS active site stabilized only the altered, transition state configuration of the α-phosphate group, one might expect to see a lag corresponding to the depletion of AQP, followed by rapid formation of ^{32}P ATP. This does not occur, implying that the interaction of AQP with TrpRS precludes its acting as a substrate. We suggest two, mutually complementary, reasons for this. First, excluding the divalent metal from the active site precludes a catalytic role with AQP. Second, the superimposed structures in Figure 7a suggest that the scrunched tetraphosphate, having already positioned the adenosine and PPi moieties to approximate the transition state configurations recognized by TrpRS, has insufficient room in the active site to expand and break the Pα-Pβ linkage.

How does Mg^{++} accelerate phosphoryl transfer?

Detailed empirical valence bond (EVB) simulations of two nuclease mechanisms [34], indicated that the electrostatic interactions with Mg^{++} contribute >10 orders of magnitude in rate enhancement in the phosphodiester hydrolysis catalyzed by enzymes using both one [35] and two [36] Mg^{++} ions. In light of that estimate, it is somewhat startling that Mg^{++} accelerates uncatalyzed phosphoryl-transfer reactions by a factor of only two or three [1; 31; 43].

Numerous reports suggest that Mg^{++} ion plays similar roles in the mechanisms of aaRS. Previous estimates for TrpRS catalysis [11] suggested that Mg^{++} ion accelerates the catalyzed reaction by a factor of at least a hundred. However, it is surprisingly difficult to exclude Mg^{++} from assays. We therefore have repeated the experiments described by Retailleau, et al., using buffers and ATP scrubbed with Chelex 100 [37] and then supplemented with increasing concentrations to 5 mM EDTA. Equilibrium calculations indicate that under these conditions, the free [Mg^{++}] should be less than 0.01 nM, while the Km for Mg^{++} is around 2 μM [11]. At the highest EDTA levels, TrpRS activity plateaus at rates about 4 orders of magnitude slower than that with Mg^{++}. The divalent metal therefore appears to contribute substantially to the TrpRS transition stabilization free energy.

The contrast between the strong dependence of aaRS catalysis on Mg^{++} and its minimal impact on the uncatalyzed rate implies that the protein itself must link the Mg^{++} mechanistically to the transition state. The TrpRS active-site Mg^{++} configuration compounds the question: no active-site residues interact directly with the Mg^{++} ion in any of the ground-state structures, although simulations suggest that Q9 may play a role in the transition state Mg^{++} configuration (H. Hu, personal communication).

We recently identified a “minimal catalytic domain”, MCD, in the TrpRS Rossmann dinucleotide binding fold, which we have excised and engineered for stability [2]. This 130-residue fragment includes all but one of the residues (K111) that interact with the two substrates. It catalyzes tryptophan activation roughly 5 orders of magnitude more slowly than the intact protein. Transition state stabilization of 10^9-fold by the MCD is comparable to that from the metal in nuclease reactions [34]. A reasonable inference is that the rudimentary MCD active-site, while providing no direct linkage to Mg^{++}, nonetheless provides an environment in which electrostatic catalysis can function at a significant level. The functional linkage between the protein and Mg^{++}, therefore, depends strongly on as yet unspecified interactions within the active site.

How does Mg^{++} interact with other potential sources of electrostatic catalysis present in TrpRS?

Figure 8 shows a transition-state model derived from the AQP:TrpRS complex coordinates. The pyrophosphate atoms and the AMP moiety are taken directly from the γ- and δ- phosphate groups and adenosine of AQP; the α-phosphate was converted to a metaphosphate. The Mg^{++} ion was located to equilibrate its average distances from surrounding coordinating groups.

Admiraal and Herschlag [1] describe five characteristics of the dissociative character in the uncatalyzed transition state for terminal phosphate hydrolysis, [1]. Uncatalyzed pyrophosphoryl transfer, associated with synthetic reactions like amino acid activation, proceed by a transition state with somewhat less dissociative character than the terminal phosphate hydrolysis ([38]; D. Herschlag, personal communication). The TrpRS active site in the AQP complex nevertheless reflects each of the following properties:

i. The nucleophile is little changed between ground state and transition state— Warshel [34] argues from simulations that the hydroxy nucleophile in hydrolytic cleavage of phosphodiester bonds must be stabilized, and implicates the metal in this role in both single and two-metal mechanisms. The tryptophan carboxylate nucleophile is 4 orders of magnitude more acidic than water, and therefore requires correspondingly less electrostatic stabilization. The hydrogen-bonding arrangement involving Y125, Water W613, the Mg^{++}, and the tryptophan αNH2 group all appear to influence the electronic configuration of one carboxylate oxygen atom (arbitrarily O_2) in such a way that the other oxygen atom can serve more effectively as the nucleophile (Figure 8a). The NH2 group may ensure that the tyrosine hydroxyl group serves as a hydrogen bond donor to the O_2 atom, while the polarity of W613 imposed by its proximity to the catalytic Mg^{++} ion ensure that the O_2 atom remains conjugated, freeing the O_1 pi electrons for nucleophilic attack. The Mg^{++} may, therefore indirectly sustain the requisite properties of the inline carboxylate oxygen, in keeping with [34] (Figure 8a).

Notably, however, the tryptophan subsite undergoes little, if any rearrangement throughout the known catalytic cycle, from which we infer that there is little modulation of the nucleophile, consistent with (i).

ii. The nonbridging oxygen atoms of the chemically changing phosphoryl group (Pα in this case) show a modest *decrease* in electron density—Although the O1α atom interacts with the Mg^{++} ion, the non-bridging oxygen atoms of the α-phosphate in Figure 8b do not interact with any active-site cationic residues that might further stabilize increased negative charge. The sole polar interaction from the protein that appears poised to assume such a role is the backbone amide nitrogen of Q9. This group would form a better hydrogen bond to the non-bridging α-phosphate oxygen, O2α, as the three phosphate oxygen atoms become planar in either a metaphosphate or pentavalent phosphate transition state. Indeed, this interaction is reminiscent of the use of backbone amide groups to form the “oxyanion hole” in serine proteases [39]. The electostatic neutrality of this group, however, is consistent with (ii)

iii. The bridging oxygen atom of the leaving group develops the greatest increase in negative charge—In contrast to the relative lack of attention to the α-phosphate, the similar positions of the β-phosphate of AQP and the Mg^{++} position in the PreTS state suggest that the Mg^{++} ion is potentially suited to compensate increased negative charge on the oxygen bridging the α and β -phosphates of ATP. Interactions with the bridging oxygen atom in the scissile bond also include a contact (2.9 Å) with Nδ2 of N18 in the TIGN signature and one (3.0 Å) with Nζ of K195 in the KMSKS signature. The special potential focus on this bridging oxygen atom is in keeping with the expectation that it develops the greatest increase in negative charge in the transition state (iii).

iv. Modest *increases* in negative charge develop on the non-bridging oxygen atoms of the leaving group—Groups arrayed about the γ- and δ-phosphates of AQP (K111, K192, K195, S194, S196; Figure 8b), and in particular the novelty of the interaction of S194 with the γ-phosphate, provide considerable evidence that were the PPi leaving group of ATP to move into the same position as the γ-δ phosphate groups of AQP, the PPi binding subsite would stabilize increased negative charge on the leaving group. T15 from the TIGN signature also interacts via a conserved, bound water molecule with the non-bridging oxygen O2β (2.9 Å). This notable interaction could donate a proton to the newly-formed PPi. These multiple electropositive interactions are all consistent with (iv).

v. Items (ii), (iii), and (iv) together imply that the change in electrostatic potential between ground state and transition state is dipolar—For amino acid activation, the α-phosphate becomes relatively more positive, the PPi leaving group more negative, relative to the ground state. The graphic representation of the electrostatic field in the active site (Figs.

8 and 9) reveals that the immediate environment of the scissile bond is indeed complementary to a dipolar transition state. The minus charges on D146 and the Tryptophan carboxylate provide a negative field proximal to the α-phosphate and on the face of the metaphosphate facing the nucleophile, while the plus charges of basic residues just enumerated provide a positive field around the leaving group, consistent with (v).

Do TrpRS:AQP interactions resemble any that accelerate amino acid activation?

The 10^5-fold activity deficit in the MCD implies additional interactions between the active site and the other parts of the protein, which alter either the structure of the MCD active site, or how it functions, or both. If, as we suggested above, the TrpRS MCD provides a rudimentary environment facilitating electrostatic catalysis by Mg^{++}, the remainder of the protein must enhance that rate by five orders of magnitude by some sort of fine-tuning, which may complement and "supercharge" the catalytic effect of the Mg^{++}. The AQP thermodynamics and structure shed new light on the possible nature of this amplified catalytic contribution in the intact protein.

The affinity of TrpRS for AQP falls short of values observed for close transition state mimics of other reactions [25]. Moreover, the geometry and charge distribution of the configurations immediately surrounding the scissile bond are radically different in AQP and in the putative transition state derived from Mg^{++}•ATP. The α-phosphate has a ground state configuration, while the bound form significantly distorts the charge distribution expected from the transition state Mg^{++}•ATP configuration. Yet, AQP binding is 200-fold tighter than ATP and results directly in crystals nearly isomorphous to those of the Pre-transition state complexes reported previously [11].

The energetics of the dramatic differences between the AQP β-phosphate and the Mg^{++} ion cannot be evaluated on the basis of data reported here. It is likely, however, that since the β-phosphate cannot mimic anything like a transition state configuration, its interactions with TrpRS contribute unfavourably to the AQP binding affinity. If the 200-fold greater affinity of AQP does, as we believe, represent binding interactions similar to those in the transition state, these must lie elsewhere in the complex. To what extent, then, might AQP resemble the transition state?

The additional β-phosphate group in AQP has a distinctive structural consequence: it pushes the terminal PPi mimic and the α-phosphate away from each other by approximately the amount expected for a transition state with dissociative character (Figure 7a). Mimicking that separation, drives the adenosine and PPi moieties them deeper into binding pockets on opposite sides of the domain boundary, the adenosine toward the Rossmann fold and the PPi toward the KMSKS loop and C-terminal anticodon-binding domain, where each benefits from enhanced binding interactions. The γ- and δ- phosphate groups of the PPi mimic intensify all of the interactions seen between the KMSKS loop and the β- and γ- phosphates of the PPi leaving group of ATP, and a new interaction develops from S194 of the KMSKS loop. These and corresponding interactions to the adenosine are strengthened (Table 3). The 200-fold greater affinity of AQP, relative to Mg^{++}•ATP, suggests that these distributed interactions must be strong enough to compensate for the unfavourable electrostatic substitutions near the α-phosphate *plus ~-3.2 Kcal/mole of additional binding free energy*. Complementarity of the active site to the actual transition state may therefore be extensively delocalized into the TrpRS adenosine- and PPi-binding subsites, as suggested by the TyrRS mutational and kinetic studies.

AQP appears to meet in a novel way the usual criteria for a transition state mimic

—AQP is not a substrate. It binds to TrpRS with substantially higher affinity than does ATP. It interacts with the active site in a manner suggesting the distributed origins of enhanced transition state affinity. TrpRS responds to the altered configurations of adenosine and the PPi

mimic by enhancing previously identified interactions to ATP and by forming novel binding interactions. Table 3 documents that the active site closes more or less uniformly on the inhibitor. The broad distribution of interactions responsible for the higher affinity of AQP throughout the adenine nucleotide binding subsites is fully consistent with the extensive mutational data for the homologous TyrRS system [8], which implicated comparable interactions in transition state binding. Both the high binding affinity of AQP and the crystal structure therefore verify in unexpected detail many expectations for a transition state in which transient, strong binding to the adenosine and PPi moieties are important for transition state stabilization.

In summary, introduction of the β-phosphate between Pα and the PPi leaving group lengthens the distance between the leaving group and Pα, moving the former into the KMSKS loop and the latter toward the nucleophile. The resulting configuration strengthens a variety of distributed binding interactions that, we suggest, contribute to transition state stabilization.

What is the role of domain motion?

The free energy cost of induced-fit, +3.0 Kcal/mole, measured for the first time in this work, is quite substantial. It represents a stored free energy that is roughly half that for the reduction in catalysis by the MCD. How might it be utilized during catalysis?

A partial, qualitative, solution to this puzzle emerged from MD simulations, which revealed a significant interaction between the PPi oxygen distances to Mg^{++} and to the ε-NH2 groups of K111 and K192 [28], implicating that interaction directly in the endergonic twist angle between domains in the PreTS state. The exergonic untwisting domain motion observed in the Products conformation [40; 41], and the strengthening of interactions to PPi in the AQP complex demonstrated here imply that breaking the bond between the bridging oxygen atom and the α-phosphorus would allow the leaving group to form stronger bonds to the KMSKS loop as it rotates away from the α-phosphate, likely accompanied by the Mg^{++} ion, which is not present in the Product complex with Trp-5′AMP [13; 15].

Moreover, the domain reorientation associated with AQP binding, which rotates the KMSKS loop toward the Products conformation, is exergonic [28]. Two reinforcing effects therefore contribute to higher AQP affinity; the separated adenosine and PPi fit better into their respective binding subsites, and the enabling domain reorientation is energetically favorable.

Loss of the twist takes the ribose and PPi-binding subsites in opposite directions, suggesting an element of strain in the catalytic mechanism. The structural reorganization of the TrpRS active site, in the conversion of the PreTS to the Products conformation via the intermediate AQP-bound state suggests that relocation of the leaving group could occur prior to the approach of the nucleophile, as in a fully dissociative transition state. The problem with this notion is the well-known presumption that protein conformations are stabilized by non-bonded interactions far too weak to distort chemical bonds [42]. Essentially, this argument is that van der Waals forces change rapidly with distance, so strain can be relaxed by small atomic movements.

The development of incremental binding energy in the AQP complex suggests a novel formulation of the strain that is not vitiated by the argument of Levitt and Warshel. Coordinated increases in binding to the dissociating pyrophosphate leaving group, coupled to its mechanical relocation can effectively strain the Pα-Pβ linkage statistically, by selecting those bond-length fluctuations that lead to bond breaking without actually changing equilibrium bond distances. By coupling the unfavorable free energy changes associated with the induced-fit to the stronger binding interactions to the dissociated leaving group, the domain relocation therefore could have a significant catalytic effect.

Do Class I and Class II aaRS use different mechanisms?

The distinction between the class-defining consensus motifs, HIGH and KMSKS for class I [43]44 45, and motifs 2 and 3 for class II, [46], probably reflects differences in the detailed mechanism by which they catalyze phosphoryl transfer. Class II aaRS appear poised to stabilize developing negative charges on the non-bridging oxygen atoms in a pentavalent α-phosphate group using a conserved arginine residue from Motif 2. Moreover, Class II active sites do not provide an extensive, mobile binding site for the PPi leaving group, whose negative charges appear to be neutralized primarily by multiple Mg^{++} ions coordinated by active-site glutamic acid residues [47; 48; 49]. This arrangement is reminiscent of that in the "two-Mg^{++} mechanism" suggested for the analogous synthetic reaction carried out by nucleic acid polymerases [36] and the associated exonucleolytic reaction [50].

In most class I active sites, on the other hand, the KMSKS loop has been implicated by mutational [7; 8; 51] and structural [52; 53] studies as a (dynamic) binding site for the pyrophosphate leaving group. Further, the KMSKS loop weakens ATP binding in the pre-transition state ground state, while strengthening transition-state binding [28; 51; 54]. Thus, conserved lysine residues and a single Mg^{++} ion in Class I active sites play slightly different roles to those played by conserved arginines and multiple Mg^{++} ions in Class II enzymes. Mg^{++} therefore must function somewhat differently in class I (1 Mg^{++}) and class II (2-3 Mg^{++}) aaRS.

An important consequence is that there is likely a requirement for the single Mg^{++} ion in Class I mechanisms to be more mobile than the multiple metals in Class II acive sites, consistent with the absence of protein ligands and the previously observed weakening of Mg^{++}-phosphate oxygen interactions by lysine ε-amino groups observed in TrpRS [28].

There are two exceptions to the Class I pattern in which the second lysine is missing from the KMSKS signature. Arginyl-tRNA synthetases provide a second lysine from upstream of the HIGH signature [16]. Eukaryotic cytoplasmic TrpRSs provide instead an arginine from a similar position homologous to Q9 [55]. In these enzymes, this upstream arginine residue might help stabilize a pentavalent phosphoryl moiety, rather than the metaphosphate that appears more appropriate in *B. stearothermophilus* TrpRS.

Concluding remarks

The path actually taken by a particular enzymatic or non-enzymatic system through the two-dimensional surface of bond-breaking and bond-making is difficult to determine, but can be studied experimentally by kinetic isotope effects [56; 57], and theoretically by quantum-mechanical simulations [58; 59]. In particular, the low-energy path may depend critically on the balance between the electrostatic charges developed on the participants and the ability of the environment (solution or enzymatic) to complement it [6]. Release of pyrophosphate in biosynthetic reactions can generate altered negative charges on a relatively large number of phosphate oxygen atoms, making such determination especially difficult. For this reason, any conclusion regarding the precise nature of the transition state for tryptophan activation by TrpRS must remain speculative without further experimental and computational work. The data reported here underscore the importance of doing such studies.

The affinity of a transition state analog should respond in the same way as the enzymatic rate to any perturbation that changes the rate [23], leading to a linear free energy relation. An orthogonal experimental test of the extent to which AQP mimics the transition state would thus be to measure AQP affinity for a range of variant TrpRSs with different activities. The activity of the TrpRS MCD is reduced by ~5 orders of magnitude [2]. This fragment should not be inhibited by AQP, because the free AQP concentration cannot be increased by that relative amount. Within the range between native TrpRS and its minimal catalytic domain lie a number

of engineered fragments and point mutants with different specific activities. It should therefore be possible to compare the AQP affinity and activity of such variants, along lines suggested by Wolfenden [23].

Experimental Procedures

Determination of Ki for AQP

Pyrophosphate exchange assays were performed as described previously [11]. Assays at AQP concentrations of 4×10^{-4} M, and 8×10^{-3} M were analyzed to determine the inhibition constant.

Synthesis, purification, and isothermal titration calorimetric analysis of Adenosine tetraphosphate (AQP)

When this work started, adenosine tetraphosphate (AQP) was commercially available from SIGMA Biochemical (A 4636), and that material was used for all crystallographic experiments and the determination of the inhibition constant, Ki. Once it became clear that AQP represented a potential transition state analog inhibitor, we were unable to purchase more compound. Subsequent titration experiments were therefore carried out using material we synthesized as follows. The ribonucleotide, 2′,3′isopropylidineadenosine (SIGMA I 4002; Aldrich 1-2,240-4) was rendered anhydrous by five repeated evaporations of anhydrous dimethylformamide (DMF; Aldrich 22,705-6) and was subsequently maintained under dried (P_2O_5) nitrogen. The anhydrous nucleotide (0.641 g, 2 mmol) was dissolved in 5 ml of anhydrous DMF and treated with 1.135 g (7 mmol) of of 1,1′-carbonyldiimidazole (Aldrich 11,553-3) in 10 ml of anhydrous DMF and maintained under dried Nitrogen for twelve h, followed by treatment with 21 ml of methanol. After 30 minutes, the solution was treated with 13.07 g (10 mmol) tetrabutylammonium tetraphosphate (prepared from Ca_2-tetraphosphate, City Chemicals 59415-82-6 by ion exchange chromatography) in 20 ml of anhydrous DMF and maintained under anhydrous conditions for 24 h.

The crude 2′,3′ isopropyllidineadenosinetetraphosphate was filtered, evaporated to dryness, and deblocked using 10% (v/v) triflouroacetic acid/water for 12 h. The tetraphosphate was purified from less highly charged components using ion-exclusion chromatography on Dowex 50W-X4-400 [60]. Subsequent purification was achieved by adsorption to acid-washed charcoal and elution at 55° C with pyridine. The resulting compound was characterized, relative to a commercial sample of AQP, ATP, and ADP by thin-layer chromatography on DEAE cellulose plates using 1.0 M phosphate, pH=3.4, and on Silica gel plates in ethanol:NH3:water, 90:1:9. AQP concentration was determined using ε_{254} = 15,400/Mol.

Isothermal titration calorimetry with AQP was performed using a Microcal VP-ITC calorimeter at two different concentrations of ligand (2.4×10^{-4} M, 8.5×10^{-5} M) and protein (6×10^{-6} M, 6×10^{-5} M) and corrected for dilution of macromolecule and ligand by separate titrations.

Crystallography of the TrpRS:AQP complex

Recombinant native and selenomethionylated TrpRS of *Bacillus stearothermophilus* were overexpressed in *Escherichia coli* and purified as previously described [12]. Binary native complex crystals were grown by microdialysis (5μL of 4mg/mL protein *vs* 2000 mL well). The protein stock buffer (0.6M potassium phosphate solution in the presence of 50%v/v glycerol) was then extensively exchanged by a precipitant solution containing only ~1M sodium citrate at pH 7.5, 10 mM $MgCl_2$ and 10 mM (freshly in solution) tri (cyclohexylammonium) adenosine 5′ tetraphosphate (AQP) (commercial source SIGMA). One mono crystal appeared within two weeks and then grew rapidly to suitable dimension 0.3 × 0.3 × 0.3 mm for X-ray diffraction experiment. Prior to the flash-cooling performed directly in the stream of liquid nitrogen at 100 K, the crystal was quickly dipped into a 15% v/v glycerol cryoprotectant solution

containing 0.1M Cæsium chloride. Refined value for crystal mosaicity during data reduction was equal to 0.56°.

Data were recorded on a RAXIS-RIGAKU IV setup, at the copper K_α wavelength, using a 18 cm Mar image plate, in a single sweep of 70 images with 1° of oscillation. Diffraction data were processed using the *HKL* package [61] (see Table 1 for statistics). Dataset was 95 % complete to 2.5 Å but the reflections in the last resolution shell present an average I/σ of 2.0 (between 2.59 and 2. 5 Å) and a $R_{sym} > 0.5$.

Native and derivative structure-factor amplitudes were calculated using *TRUNCATE* 62 63 and then derivative amplitudes were scaled relative to the natives between 10 and 4.0 Å using the program *SCALEIT* 64, [63]. Later, more redundant and higher resolution data were collected from a selenomethionylated crystal complexed with an adenosine nucleotide using the same X-ray diffraction setup (see Table 4). This potential derivative crystal turned out to be more isomorphous with the native AQP complex than former ATP complex crystals ($R_{ISO} = 0.163$ *vs* 0.428 see Table 4) and therefore was useful for IR phasing method.

Molecular replacement using the AMoRe software [65] was then used to place a model (protein atoms from 1M83) in the asymmetric unit. The best solution by far, obtained after search of rotation function then translation function using X-ray data from 8 to 4 Å resolution had a structure factor correlation coefficient of 69.0 and an R-factor of 33.3 %. The output coordinates were divided into five pieces (RF - α-helix A (residues 1-15 and 30-165), α-helix A, (residues 16-29), long belt (residues 166-199), SD (residues 200-265), helical long path (residues 266-328) and subjected to a rigid-body fitting using the adequate macro in *CNS* 66: R-factor decreased from 49% to 44% after significant reorientation of the SD with respect to the RF. Phases derived from the fitting coordinates were then used to calculate isomorphous and anomalous difference Fourier maps to locate positions of heavy atoms.

Phasing was provided by isomorphous differences for nine of ten Se-S atoms, plus one cæsium cation whose atomic coordinates were input into *SHARP* 67 to start heavy-atom parameter refinement for SIR phasing. The weak anomalous signal was also treated by refining scattering factors for Se-S and Cs at the Cu Kα wavelength. SIR(AS) phases were derived to 2.5Å with overall figures of merit > 0.3 (see Table 5). Phase quality was sufficient to draw an accurate molecular envelope that permitted solvent-density modification (SOLOMON) [68], as implemented within *SHARP*, to output a detailed electron density map using an optimized starting solvent fraction of 48.7%. The quality of this 2.5Å map was assessed by the autotracing of about 90 % of the protein backbone model in 120 cycles by the *wARPNtrace* protocol [69] through the interface with *SHARP*. Attempts of sidechain docking with respect to the sequence were performed every 15 cycles and geometry adjustments were done by *REFMAC* 70 and constrained by the *SHARP* phase distribution.

Further, structure solution was achieved using the program *BUSTER* 71; [72] and interfaced with *TNT* 73. The core of this program implements statistical treatment of both experimental and model structure factors according to the maximum-likelihood and maximum-entropy methods [71]. The first part of the process was driven by the maximum likelihood refinement of the atomic parameters of the incomplete {poly-Gly, -Ala, -Ser} ArpWarp model. SIR(AS) phase information output by SHARP as the Hendrickson-Lattman coefficients constrained the partial structure refinement whose stereochemical and geometrical restraints were handled in TNT.

During the atomic parameter refinement process, bulk solvent and the random distribution of missing atoms were kept fixed. The missing atoms were utilized as model-based non-uniform prior to output low-resolution distributions and together with the bulk solvent envelope and the fragment model, accounted for the real-space picture of the crystal content. Maximum-

entropy modulation of the envelope for missing atoms aims at recovering accurate density in their expected regions.

Although measured amplitudes did not exceed 2.5Å of resolution, the overlapped part of |2Fo-Fc, $\Phi_{\text{refined model}}$| and |Fo-Fc, $\Phi_{\text{refined model}}$| electron densities that delineates the solvent boundary was checked continuously during the refinement process for strongly protein-bound molecules. Few (55) waters were included in the model with confidence, as they were (for most of them) already present in the 2.2Å ATP complex, id PDB code 1M83.

The AQP was refined with restrained topology and parameter files established by *xplo2d* 74 and atomic B-factors were kept correlated. At the end of the refinement, ligand occupancy was refined until convergence after keeping all coordinates and atomic B-values fixed, those for the ligand were set equal to the overall B-value of the protein region surrounding the ligand. Refinement came up with an occupancy value of 0.85. This was followed by another round B-factor refinement (overall value nearly the same as the protein backbone), individual atomic values increasing toward the flexible phosphate tail, attaining almost 60 $Å^2$ for the δ-phosphate.

Two catalytic water molecules, the one (5σ) that interacts with the hydroxyl group O3′ of the ribose and that (6.5σ) which bridges the hydroxyl of Thr15 with an oxygen of a nucleotide phosphate (beta-phosphate in the ATP binary complex) were not among the top list peaks in the difference Fo-Fc Fourier map after protein model completion. They were nevertheless conserved in the final model with B-factor values refined to reasonable values (< 47 $Å^2$).

On the top of the list was a strong, round (12σ) peak of density showing up in the cationic site previously noticed [15]. This was modelled as a caesium cation that diffused during crystal post-soaking. A low occupancy (0.3) was attributed to this very heavy atom element to comply with the *SHARP* refinement statistics and also with a reasonable value of refined thermal parameter. Its coordination sphere is four in this complex, making short interactions (≤ 3.5Å) with three carbonyl oxygen atoms of Gln 30, 33 and 74. Gln74 and Asn34 amide groups, sulphur atoms from Met 1 (and possibly that of Cys 35) are also in the vicinity of the cation. The potential of this site to offer variable coordination sphere and chemical nature of neighbours, O, N or S suggests that a large variety of cations could be accommodated, and we previously have identified K^+ at this site in crystals grown from potassium salts. However, the present result contrasts to some extent with weak evidence for sodium binding in the binary ATP complex crystallized in sodium citrate. Although this cation function is likely to be structural (This site is located far from the adenylation site, in the first half of the RF domain in a pocket created by two helices that connect the C-terminus of helix αA to the β-brand B on one side and the C-terminus of helix αB to the β-strand C on the other (see Fig 3)), (either mono or di-valent?) metal-dependent activities of *B. stearothermophilus* TrpRS should be worth being investigated.

Another residual, significant (9σ) feature in the Fourier difference was located in the tryptophan-binding pocket, addressing again the issue of contamination of the Trp pocket. This density was fitted as hexylammonium, the counterion of commercially supplied AQP, the aliphatic group within the hydrophobic cavity, while the carboxylic group of the Trp-binding determinant, Asp132 directed to the ammonium group.

Statistics at the completion of the model refinement are given in Table 6. The final crystallographic R-free is equal to 25.8 for and the R-factor is 19.1 for all data between 20.0 and 2.5 Å resolution. The standard deviation on coordinates estimated from the Cruickshank approach within SFCHECK [75] is 0.5 Å. Agreement between the model and the *SIGMAA* 2Fo-Fc final map is assessed by an overall real-space correlation coefficient of 0.85 calculated by the macro rs_fit within *O*. A plot of these coefficients for each residue is displayed in Figure 1 in relation with the corresponding main chain temperature factors. Geometry of the model

was analysed by *PROCHECK* 76, revealing that almost 93% of residues in the structure are in the most favoured regions of the Ramachandran plot (Figure 2). The coordinates for the binary complex of the AQP:TrpRS of *B. stearothermophilus* and the observed structure factors as well have been deposited with the Protein Data bank, identification code xxx.

For purposes of coordinate comparisons, all the models were superimposed by *LSQKAB* using 42 C^{α} atoms taken from the first half of the RF domain, which has been used as a reference orientation for previous comparisons among class I aaRSs (Doublié *et al*, 1995). Color figures were prepared using MOLSCRIPT [77] rendered by RASTER3D [78] and PYMOL [79].

Acknowledgments

This work was supported by NIGMS-48519. We are grateful also to Globalphasing ltd for licenses for SHARP and BUSTER/TNT and for their assistance. We gratefully acknowledge substantive discussions with Barry Lentz and Jan Hermans, which clarified several important issues addressed in determining AQP affinity; with Hao Hu for discussion of his unpublished quantum mechanical and MD simulations; and we thank Eric First, Dan Herschlag, Gordon Hammes, Chris Halkides, Jan Hermans, and Richard Wolfenden for their comments on the manuscript. Several reviewers made key suggestions that improved the presentation.

References

1. Admiraal SJ, Herschlag D. Mapping the transition state for ATP hydrolysis: implications for enzymatic catalysis. Chem Biol 1995;2:729–39. [PubMed: 9383480]
2. Pham Y, Li L, Kim A, Weinreb V, Butterfosss G, Kuhlman B, Carter CW Jr. A Fused, 130-Residue Catalytic Domain May Represent an Ancestral Class I Aminoacyl-tRNA Synthetase. 2006In preparation
3. Tetas M, Lowenstein JM. The Effect of Bivalent Metal Ions on the Hydrolysis of Adenosine Di- and Tri-Phosphates. Biochemistry 1963;2:350–357. [PubMed: 13980762]
4. Mildvan AS. Mechanisms of signaling and related enzymes. Proteins 1997;29:401–16. [PubMed: 9408938]
5. Åqvist J, Kolmodin K, Florian J, Warshel A. Mechanistic alternatives in phosphate monoester hydrolysis: what conclusions can be drawn from available experimental data? Chemistry and Biology 1999;6:R71–R80. [PubMed: 10074472]
6. Florian J, Warshel A. Phosphate Ester Hydrolysis in Aqueous Solution: Associative versus Dissociative Mechanisms. Journal of Physical Chemistry B 1998;102:719–734.
7. Fersht, A. Dissection Of The Structure And Activity Of An Enzyme. In: Kaiser, ET., editor. Design of Enzymes and Enzyme Models. Vol. XXXI. Robert A. Welch Foundation; Houston, TX: 1988. p. 159-182.
8. Fersht AR. Dissection of the structure and activity of the tyrosyl-tRNA synthetase by site-directed mutagenesis. Biochemistry 1987;26:8031–8037. [PubMed: 3442641]
9. Mechulam Y, Dardel F, LeCorre D, Blanquet S, Fayat G. Lysine 335, Part of the KMSKS Signature Sequence, Plays a Crucial Role in the Amino Acid Activation Catalyzed by the Methionyl-tRNA Synthetase from *Escherichia coli*. Journal of Molecular Biology 1991;217:465–475. [PubMed: 1847216]
10. Schmitt E, Panvert M, Blanquet S, Mechulam Y. Transition state stabilization by the 'high' motif of class I aminoacyl-tRNA synthetases: the case of *Escherichia coli* methionyl-tRNA synthetase. Nucleic Acids Research 1995;23:4793–4798. [PubMed: 8532520]
11. Retailleau P, Huang X, Yin Y, Hu M, Weinreb V, Vachette P, Vonrhein C, Bricogn G, Roversi P, Ilyin V, Carter CW Jr. Interconversion of ATP binding and conformational free energies by Tryptophanyl-tRNA Synthetase: structures of ATP bound to open and closed, pre-transition conformations. Journal of Molecular Biology 2003;325:39–63. [PubMed: 12473451]
12. Ilyin VA, Temple B, Hu M, Li G, Yin Y, Vachette P, Carter CW Jr. 2.9 A crystal structure of ligand-free tryptophanyl-tRNA synthetase: domain movements fragment the adenine nucleotide binding site. Protein Sci 2000;9:218–31. [PubMed: 10716174]

13. Doublie S, Bricogne G, Gilmore C, Carter CW Jr. Tryptophanyl-tRNA synthetase crystal structure reveals an unexpected homology to tyrosyl-tRNA synthetase. Structure 1995;3:17–31. [PubMed: 7743129]

14. Brown KA, Brick P, Blow DM. Structure of a Mutant of Tyrosyl-tRNA Synthetase with Enhanced Catalytic Properties. Nature 1987;326:416–418. [PubMed: 3104791]

15. Retailleau P, Yin Y, Hu M, Roach J, Bricogne G, Vonrhein C, Roversi P, Blanc E, Sweet RM, Carter CW Jr. High-resolution experimental phases for tryptophanyl-tRNA synthetase (TrpRS) complexed with tryptophanyl-5′AMP. Acta Crystallogr D Biol Crystallogr 2001;57:1595–608. [PubMed: 11679724]

16. Sekine, Si; Shimada, A.; Nureki, O.; Cavarelli, J.; Moras, D.; Vassylyev, DG.; Yokoyama, S. Crucial Role of the HIGH-loop Lysine for the Catalytic Activity of Arginyl-tRNA Synthetase. Journal of Biological Chemistry 2001;276:3723–3726. [PubMed: 11106639]

17. Delagoutte B, Bey G, Poch O, Moras D, Cavarelli J. Deciphering the relationships between structure, function, evolution, and sequence of arginyl-tRNA synthetases. The EMBO Journal. 2002To be published

18. Delagoutte B, Moras D, Cavarelli J. tRNA aminoacylation by arginyl-tRNA synthetase: induced conformations during substrates binding. The EMBO Journal 2000;19:5599–5610. [PubMed: 11060012]

19. Cusack S, Yaremchuk A, Tukalo M. The 2 A crystal structure of leucyl-tRNA synthetase and its complex with a leucyl-adenylate analogue. Embo J 2000;19:2351–61. [PubMed: 10811626]

20. Sekine, Si; Nureki, O.; Dubois, DY.; Bernier, S.; Chênevert, R.; LaPointe, J.; Vassylyev, DG.; Yokoyama, S. ATP Binding by glutamyl-tRNA synthetase is switched to the productive mode by tRNA binding. EMBO Journal 2003;22:676–688. [PubMed: 12554668]

21. Sekine, Si; Nureki, O.; Vassylyev, DG.; Bernier, S.; Chênevert, R.; LaPointe, J.; Yokoyama, S. Structural Basis for the tRNA-dependent Catalytic Activation of Glutamyl-tRNA Synthetase. EMBO Journal 2003;22:676–688. [PubMed: 12554668]

22. Wolfenden R. Transition State Analog Inhibitors and Enzyme Catalysis. Ann Rev Biophys Bioeng 1976;5:271–306. [PubMed: 7991]

23. Radzicka A, Wolfenden R. Transition State and Multisubstrate Analog Inhibitors. Methods in Enymology 1995;249:284–312.

24. Fersht, AR. Structure and Mechanism in Protein Science. W. H. Freeman and Company; New York: 1999.

25. Frick L, Yang C, Wolfenden R, Marquez VE. Binding of Pyrimidine-2one-Ribonucleoside by Cytidine Deaminase as the Transition State Analogue 3,4-Dihydrouridine and the Contribution of the 4-Hydroxyl Group to its Binding Affinity. Biochemistry 1989;28:9423–9430. [PubMed: 2692708]

26. Adolfson R, Moudrianakis E. Control of Complex Metal Ion Equilibria in Biochemical Reaction Systems: Intrinsic and Apparent Stability Contants of Metal Adenin Nucleotide Complexes. The Journal of Biological Chemistry 1978;253:4378–4379. [PubMed: 659423]

27. Majumbder R, Wang J, Lentz B. Effects of Water Soluble Phosphotidylserine on Bovine Factor Xa: Functional and Structural Changes Plus Dimerization. Biophysical Journal 2003;84:1238–1251. [PubMed: 12547804]

28. Kapustina M, Carter CW Jr. Computational Studies of Tryptophanyl-tRNA Synthetase: Activation of ATP by Induced-Fit. Journal of Molecular Biology 2006;362:1159–1180. [PubMed: 16949606]

29. George P, Witonsky RJ, Trachtman M, Wu X, SoeqER Q, Richman L, Shurav F, Lentz B. An Enquiry into the Importance of Solution Effects in Phosphate Ester and Anhydride Reactions. Biochimica Biophysica Acta 1970;223:1–15.

30. Yin, Y. Ph D. University of North Carolina at Chapel Hill; 1995. Crystallographic Study of *Bacillus stearothermophilus* Tryptophanyl-tRNA Synthetase in the Catalytic Reaction.

31. Wells TNC, Fersht AR. Use of Binding Energy in Catalysis Analyzed by Mutagenesis of the Tyrosyl-tRNA Synthetase. Biochemistry 1986;25:1881–1886. [PubMed: 3518794]

32. Butler PJG, Klug A. The Assembly of a Virus. Sci Am 1978;239:62–69. [PubMed: 734434]

33. Fersht AR, Knill Jones JW, Bedouelle H, Winter G. Reconstruction by site-directed mutagenesis of the transition state for the activation of tyrosine by the tyrosyl-tRNA synthetase: a mobile loop

envelopes the transition state in an induced-fit mechanism. Biochemistry 1988;27:1581–7. [PubMed: 3284584]

34. Fothergill M, Goodman M, Petruska J, Warshel A. Structure-Energy Analysis of the Role of Metal Ions in Phosphodiester Bond Hydrolysis by DNA Polymerase I. Journal of the American Chemical Society 1995;117:11619–11627.
35. Åqvist J, Warshel A. Free Energy Relationships in Metalloenzyme-Catalyzed Reactions. Calculations of the Effects of Metal Ion Substitutions in Staphylococcal Nuclease. Journal of the American Chemical Socieety 1990;112:2860–2868.
36. Beese LS, Steitz TA. Structural basis for the 3′ 5′ exonuclease activity of Escherichia coli DNA polymerase 1: a two metal ion mechanism. The EMBO Journal 1991;10:25–33. [PubMed: 1989886]
37. Holmquist B. Elimination of Metals. Methods in Enymology 1981;158:6–12.
38. Messmore JM, Raines RT. Pentavalent Organo-Vanadates as Transition-State Analogues for Phosphoryl Transfer Enzymes. Journal of the American Chemical Society 2000;122:9911–9916.
39. Robertus JD, Kraut J, Alden RA, Birktoft JJ. Subtilisin: A Sterochemical Mechanism Involving Transition State Stabilization. Biochemistry 1972;11:4293–4303. [PubMed: 5079900]
40. Doublié S, Bricogne G, Gilmore CJ, Carter CW Jr. Tryptophanyl-tRNA synthetase crystal structure reveals an unexpected homology to Tyrosyl-tRNA synthetase. Structure 1995;3:17–31. [PubMed: 7743129]
41. Retailleau P, Hu M, Bricogne G, Vonrhein C, Roversi P, Blanc E, Sweet RM, Carter CW Jr. High resolution experimental phases for Tryptophanyl-tRNA synthetase (TrpRS) complexed with Tryptophanyl-5′AMP. Acta Crystallographica 2001;D57:1595–1608.
42. Levitt M, Warshel A. Theoretical Studies of Enzymic Reactions" Dielectric, Electrostatic and Steric Stabilization of the Carbonium Ion in the Reaction of Lysozyme. Journal of Molecular Biology 1976;103:227–249. [PubMed: 985660]
43. Barker DG, Winter G. Conserved cysteine and histidine residues in the structures of the tyrosyl and methionyl-tRNA synthetases. FEBS Lett 1982;145:191–3. [PubMed: 6751870]
44. Webster T, Tsai H, Kula M, Mackie GA, Schimmel P. Specific sequence homology and three-dimensional structure of an aminoacyl transfer RNA synthetase. Science 1984;226:1315–7. [PubMed: 6390679]
45. Hountondji C, Dessen P, Blanquet S. Sequence similarities among the family of aminoacyl-tRNA synthetases. Biochimie 1986;68:1071–8. [PubMed: 3096385]
46. Eriani G, Delarue M, Poch O, Gangloff J, Moras D. Partition of tRNA synthetases into two classes based on mutually exclusive sets of sequence motifs. Nature 1990;347:203–6. [PubMed: 2203971]
47. Arnez JG, Augustine JG, Moras D, Francklyn CS. The first step of aminoacylation at the atomic level in histidyl-tRNA synthetase. Proc Natl Acad Sci USA 1997;94:7144–7149. [PubMed: 9207058]
48. Belrhali H, Yaremchuk A, Tukalo M, Berthet-Colominas C, Rasmussen B, Bosecke P, Diat O, Cusack S. The structural basis for seryl-adenylate and Ap4A synthesis by seryl- tRNA synthetase. Structure 1995;3:341–52. [PubMed: 7613865]
49. Desogus G, Todone F, Brick P, Onesti S. Active site of lysyl-tRNA synthetase: structural studies of the adenylation reaction. Biochemistry 2000;39:8418–25. [PubMed: 10913247]
50. Steitz TA, Steitz JA. A general two-metal-ion mechanism for catalytic RNA. Proc Natl Acad Sci USA 1993;90:6498–6502. [PubMed: 8341661]
51. First EA, Fersht AR. Mutational and Kinetic Analysis of a Mobile Loop in Tyrosyl-tRNA Synthetase. Biochemistry 1993;32:13658–13663. [PubMed: 8257699]
52. Carter, CW., Jr; Ilyin, VA.; Yin, Y.; Huang, X.; Retailleau, P. Using Crystallography to Understand Enzyme Mechanism. St. Paul, MN: 2002.
53. Carter, CW, Jr. Tryptophanyl-tRNA Synthetases. In: Ibba, M.; Francklyn, C.; Cusack, S., editors. The Aminoacyl-tRNA Synthetases. Landes Biosciences/ Eurekah.com; Georgetown, TX: 2005. p. 99-110.
54. First EA, Fersht AR. Analysis of the role of the KMSKS loop in the catalytic mechanism of the tyrosyl-tRNA synthetase using multimutant cycles. Biochemistry 1995;34:5030–43. [PubMed: 7711024]

55. Yang XL, Otero FJ, Skene RJ, McRee DE, Schimmel P, Ribas de Pouplana Ls. Crystal structures that suggest late development of genetic code components for differentiating aromatic side chains. Proceedings of the National Academy of Sciences, USA 2003;100:15376–15380.
56. Gerretana B, Frey PA, Cleland WW. Characterization of the Transition-State Structure of the Reaction of Kanamycin Nucleotydyltransferase by Heavy-Atom Kinetic Isotope Effects. Biochemistry 2001;40:2972–2977. [PubMed: 11258909]
57. Schramm VL. Enzymatic Transition-State Analysis and Transition-State Analogs. Methods in Enzymology 1999;308:301–355. [PubMed: 10507010]
58. Florian J, Goodman M, Warshel A. Computer Simulation of the Chemical Catalysis of DNA Polymerases: Discriminating between Alternative Nucleotide Insertion Mechanisms for T7 DNA Polymerase. Journal of the American Chemical Society 2003;125:8163–8177. [PubMed: 12837086]
59. Florian J, Goodman M, Warshel A. Computer simulations of protein functions: Searching for the molecular origin of the replication fidelity of DNA polymerases. Proceedings of the National Academy of Sciences 2005;102:6819–6824.
60. Leigh CPH, Cashion PJ. Rapid Separation of nucleoside mono-,di-, and triphosphates on ion-exlcusion/exchange columns. Journal of Chromatography 1980;192:490–493.
61. Otwinoski Z, Minor W. Processing of X-ray Diffraction Data Collected in Oscillation Mode. Meth Enzymol 1997;276:307–326.
62. French GS, Wilson KS. On the Treatment of Negative Intensity Observations. Acta Crystallographica 1978;A34:517–525.
63. CCP4. The SRC(UK) Collaborative Computing Project No 4: A Suite of Programs for Protein Crystallography. Daresbury Laboratory; Daresbury, U.K.: 1991.
64. Howell L, Smith D. Identification of heavy-atom derivatives by normal probability methods. Journal of Applied Crystallography 1992;25:81–86.
65. Navaza J. AMoRe: An Automated Molecular Replacement Package. Methods in Enymology 1997;276:581–594.
66. Brunger AT, Adams PD, Clore GM, DeLano WL, Gros P, Grosse-Kunstleve RW, Jiang JS, Kuszewski J, Nilges M, Pannu NS, Read RJ, Rice LM, Simonson T, Warren GL. Crystallography & NMR system: A new software suite for macromolecular structure determination. Acta Crystallogr D Biol Crystallogr 1998;54:905–21. [PubMed: 9757107]
67. de La Fortelle E, Bricogne G. Maximum-Likelihood Heavy-Atom Parameter Refinement for Multiple Isomorphous Replacement and Multiwavelength Anomalous Diffraction Methods. Methods in Enzymology 1997;276:472–494.
68. Abrahams JP, Leslie AGW. Methods Used in the Structure Determination of Bovine Mitochondrial F_1 ATPase. Acta Cryst 1996;D52:30–42.
69. Myers RJ, Perrakis A, Lamzin VS. ARP/wARP and Automatic Interpretation of Protein Electron Density Maps. Methods in Enymology 2003;374:229–244.
70. Murshudov GN, Vagin A, Dodson EJ. Refinemente of Macromolecular Structures by the Maximum-Likelihood Method. Acta Crystallographica D Biol Crystallogr 1997;D53:240–255.
71. Bricogne G. Bayesian Statistical Viewpoint on Structure Determination: Basic Concepts and Examples. Methods in Enzymology 1997;276:361–423.
72. Blanc E, Roversi P, Vonrhein C, Flensburg C, Lea SM, Bricogne G. Refinement of severely incomplete structures with maximum likelihood in BUSTER-TNT. Acta Crystallographica, Section D, Biological Crystallography 2004;D60:2210–2221.
73. Tronrud DE. TNT refinement package. Methods Enzymol 1997;277:306–19. [PubMed: 9379924]
74. Kleywegt GA, Jones TA. Efficient Rebuilding of Protein Structures. Acta Crystallographica 1996;D52:826–828.
75. Vaguine AA, Richelle J, Wodak SJ. SFCHECK: a unified set of procedures for evaluating the quality of macromolecular structure-factor data and their agreement with the atomic model. Acta Crystallogr D Biol Crystallogr 1999;55:191–205. [PubMed: 10089410]
76. Laskowski RA, Moss DS, Thornton JM. Main-chain bond lengths and bond angles in protein structures. J Mol Biol 1993;231:1049–67. [PubMed: 8515464]
77. Kraulis P. J Appl Cryst 1991;24:946–950.

78. Merrit EA, Murphy MEP. Acta Cryst D 1994;50:869–873. [PubMed: 15299354]
79. Delano, WF. The PYMOL Molecular Graphics System PYMOL X11 Hybrid edit. Delano Scientific; San Carlos, CA: 2002.

Abbreviations

aaRS
aminoacyl tRNA-synthetase

TrpRS
tryptophanyl tRNA-synthetase

AQP
Adenosine 5′ -tetraphosphate

ATP
Adenosine 5′-triphosphate

PPi
pyrophosphate

RMSD
root-mean-square deviation

MCD
minimal catalytic domain.

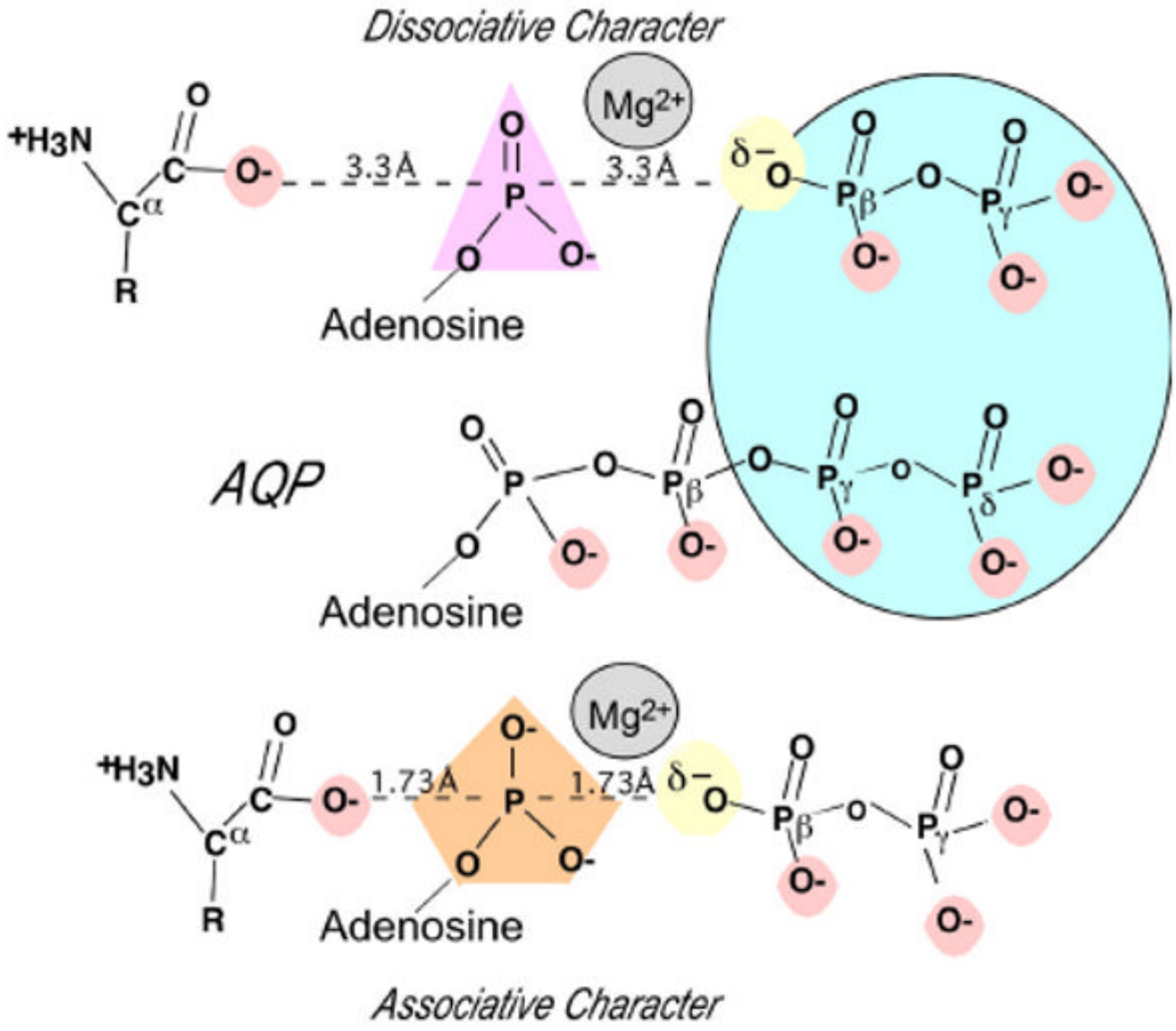

Figure 1.

Limiting transition states for phosphoryl-transfer reactions involving ATP nucleophilic displacement at Pα of ATP (after [1]). The relationship between the structure of adenosine tetraphosphate and a dissociative transition state is based on the potential equivalence of the γ- and δ- phosphates to the β- and γ- phosphates of the PPi leaving group (light blue ellipse).

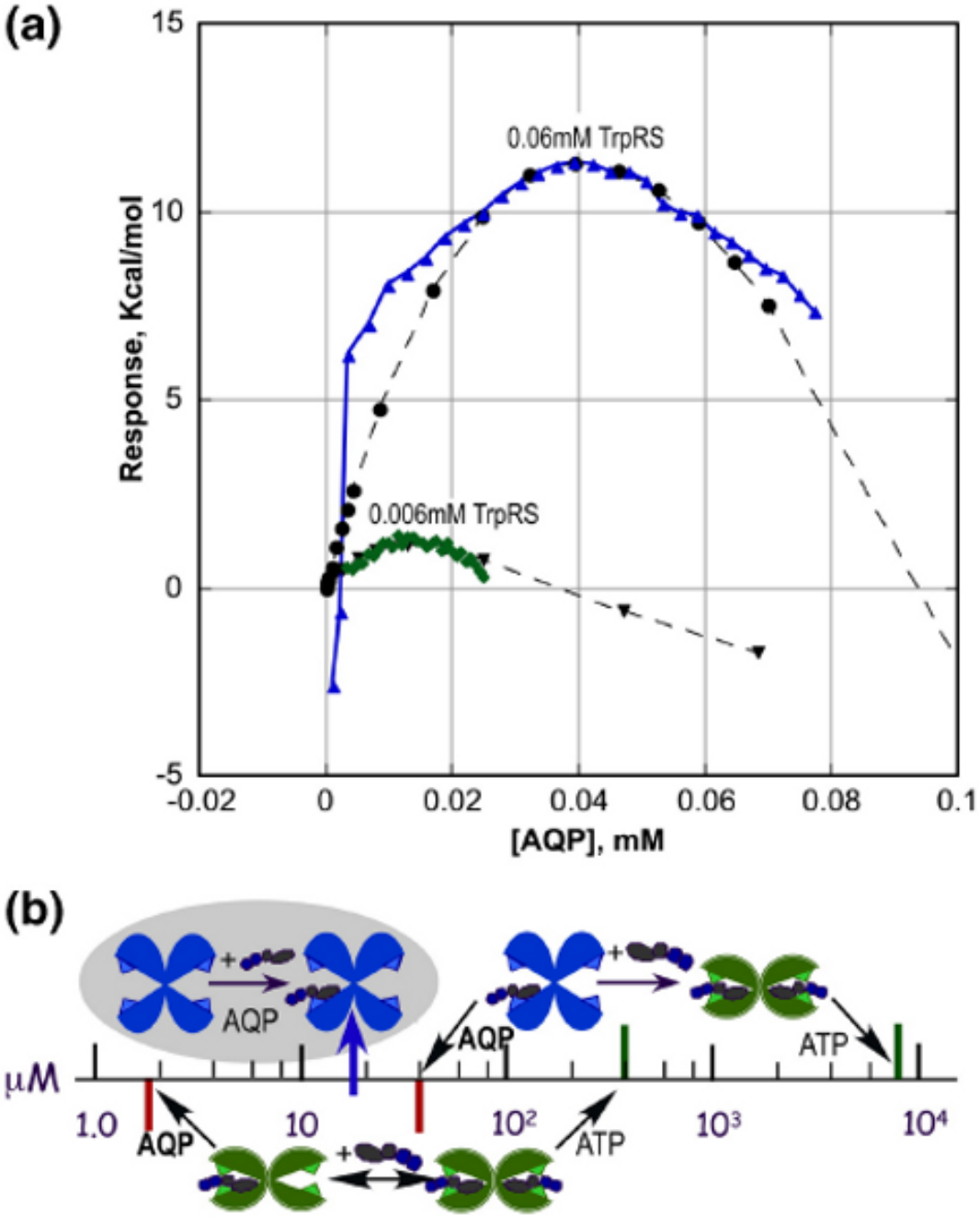

Figure 2.

Affinity measurements. **a.** Isothermal titration calorimetry. Experimental data are blue triangles for titration of 60 μM TrpRS and green diamonds for titration of 6 μM TrpRS. Black symbols and dashed lines represent the fit of the binding model whose thermodynamic parameters are in Table 1. **b.** Binding data from (**a**) in the context of other affinity determinations for AQP and ATP. The logarithmic scale represents measured dissociation constants. Three types of binding processes - exchange into assembled active sites measured by PPi exchange (Ki for AQP, Km for ATP; bold red lines below the scale, green logos), binding to the open form (bold blue arrow; shaded blue logos) and binding accompanied by induced-fit (ITC for AQP; small angle X-ray scattering for ATP [11]; bold green lines above the scale, blue to green logos) are

compared. The differential between AQP and ATP affinities is comparable in the two cases where all quantities have been determined. The same is true for the estimate of the free energy of the conformational change, given by the difference between the induced-fit and exchange dissociation constants.

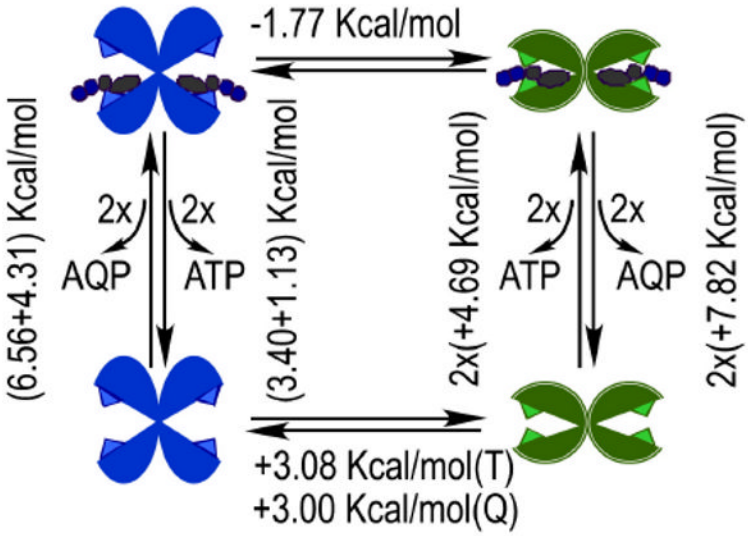

Figure 3.

Thermodynamic cycle for adenine nucleotide binding and Induced-fit conformation change. Conformational equilibria are horizontal, ligand-binding equilibria vertical. Free energies for both dissociations from the closed, PreTS conformation are identical by virtue of crystallographic symmetry. Corresponding values for the open conformation are distinct and obtained from ITC (Figure 2) and from regression analysis (Table 2), respectively, as is the free energy for the induced-fit conformational change associated with binding the second nucleotide ligand to the open conformation. Duplicate free energies are for ATP (T) and AQP (Q) binding, and the agreement for the values obtained for the two nucleotide ligands places an upper limit on the error of the assumptions.

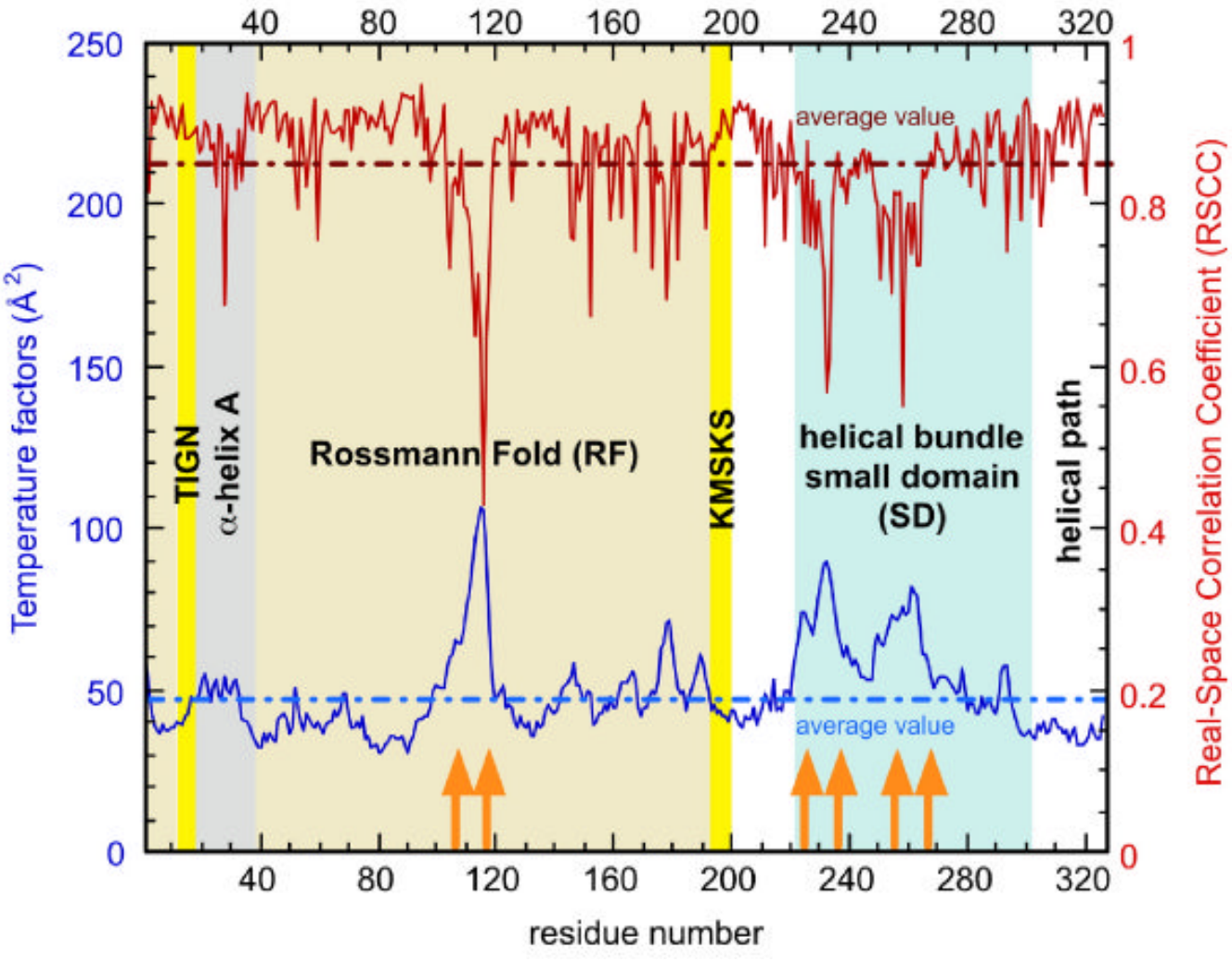

Figure 4.

Plot of the variation of the average main chain temperature factors (blue) and the real-space correlation coefficient per residue with the final SigmaA map output by O (red). The orange arrows delineate the putative anchorage sites of the tRNA.

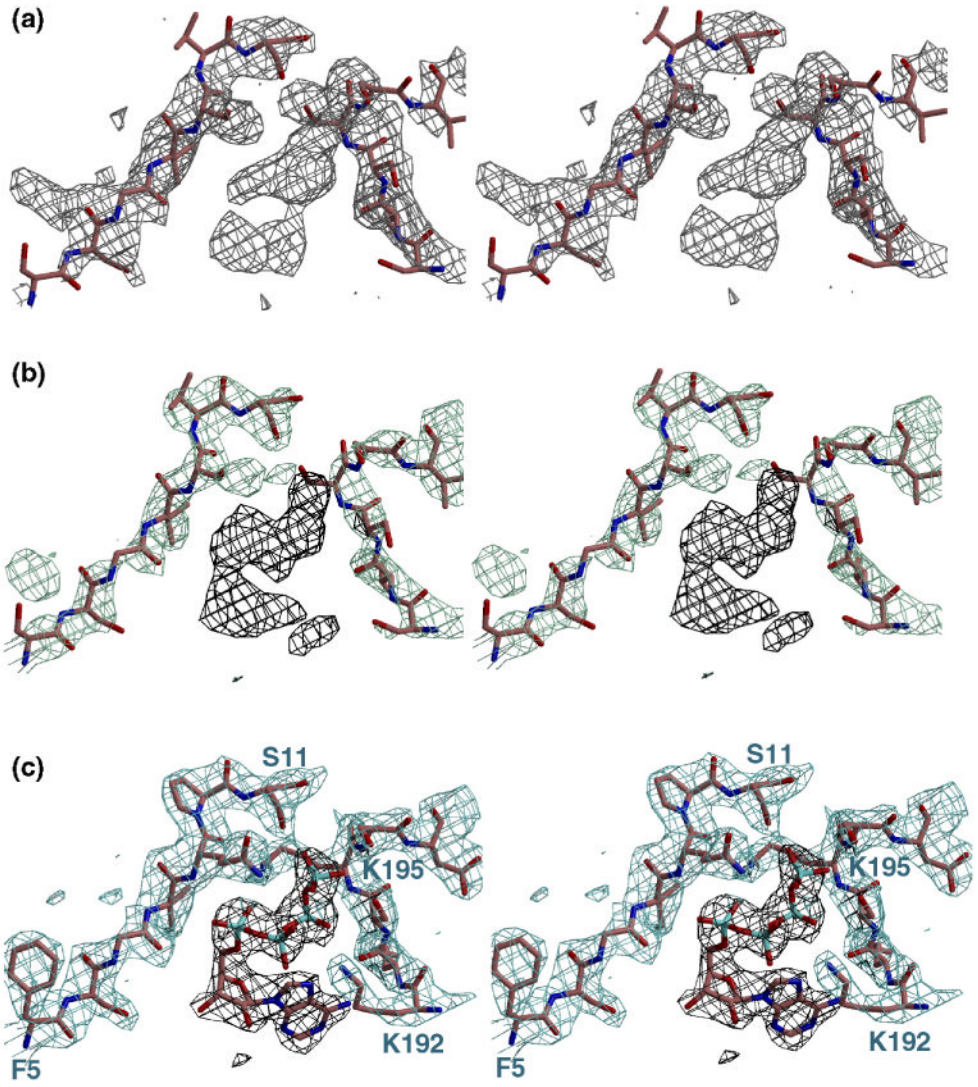

Figure 5.

Electron-density maps in the region of the nucleotide pocket superimposed with the arpwArp first model for the two first views and with the refined final model (id PDB code). These maps were calculated subsequently **(a)** with experimental SIRAS phases output by *SHARP*, **(b)** after density modification by *SOLOMON* (black contour aims at highlighting the nucleotide) and **(c)** final SIGMAA 2Fo-Fc map within *BUSTER*. Contouring level was 1.2σ except for the SOLOMON map (2σ).

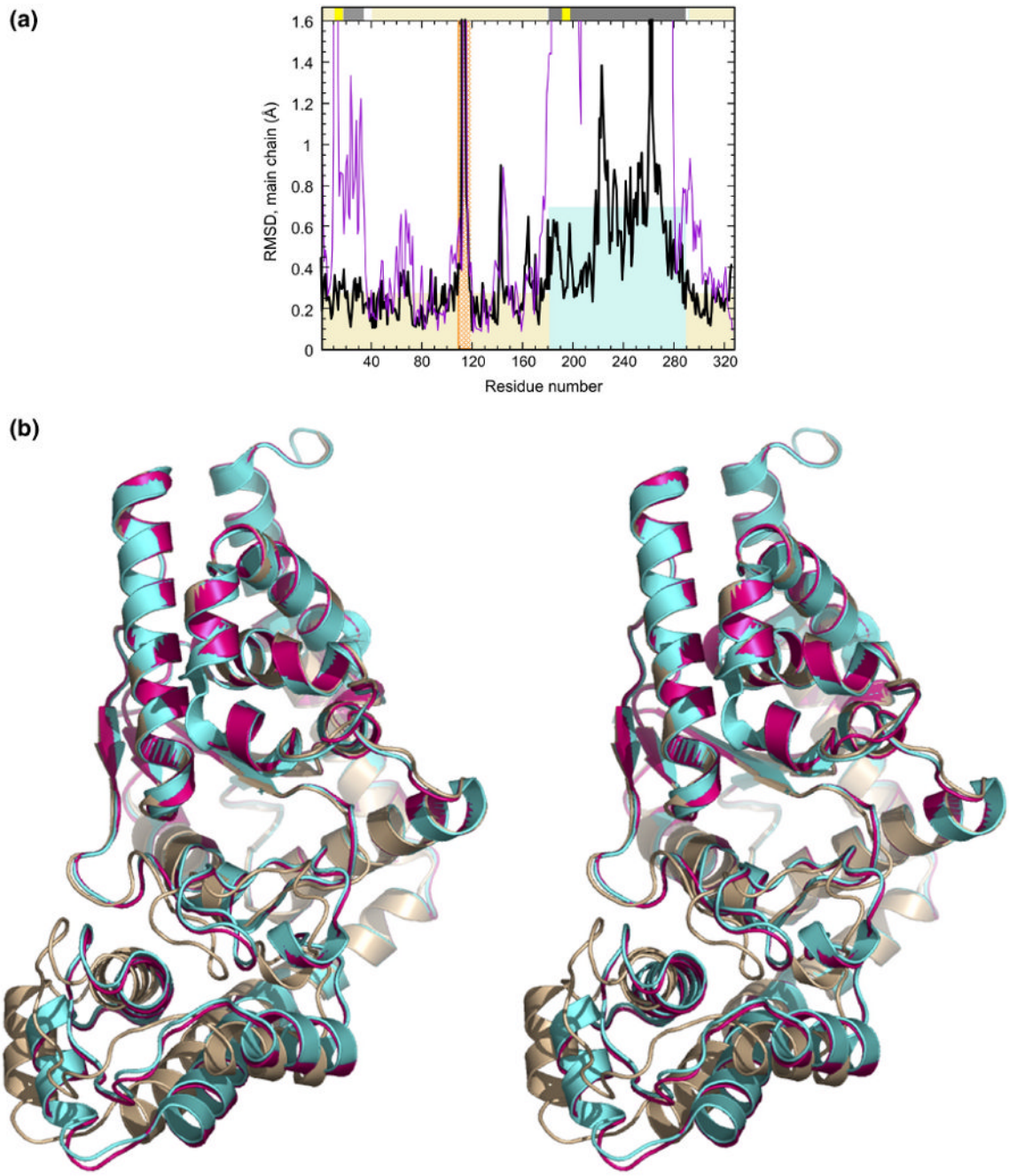

Figure 6.

a. Plot of RMSD between TrpRS:AQP coordinates and the pre-transition state complex with ATP (black) and that with the adenylate product complex (magenta). Coloured beige and gray rectangles highlight two groups of RMSD values from domains that move in opposite directions, relative to one another, in the catalytic transition. **b.** Ribbon drawing of superimposed backbones for the following monomers: cyan, ATP complex, magenta, AQP complex and wheat, the Trp-5′AMP complex. The dimer interface is at the top, and points upward and to the left.

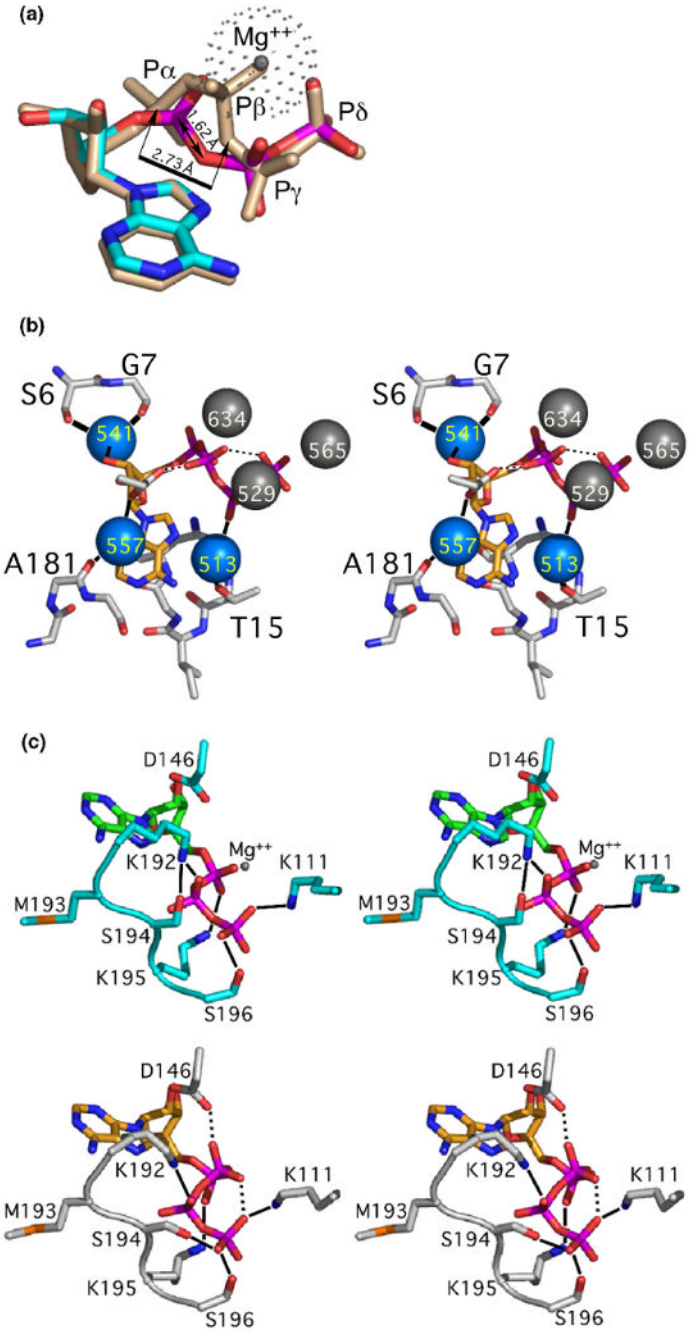

Figure 7.

Differences between the closed, pre-transition state ATP complex and the complex formed with AP4 **a.** The two ligands are superimposed and precisely aligned, once the RF domains are aligned. The adenosine, ribose and terminal pyrophosphate moieties of ATP (functional color) and AQP (wheat) compounds superimpose closely; the differences being largely in the configuration of the Pα phosphate and Mg^{++} ion in the ATP complexes and the Pα and Pβ phosphate groups of AQP. A consequence of the sequestration of the Pγ and Pδ phosphates into the pocket formed by the KMSKS loop is that the bridging oxygen atom between Pβ and Pγ (O3β) is 2.73 Å from Pα, compared to the corresponding distance in ATP (1.62 Å) **b.** Three water molecules (blue) conserved in all TrpRS crystal structures that contain the adenosine

moiety (five PreTS complexes and six Products complexes) are also preserved in the AQP complex. Three additional water molecules (gray) observed in the ATP complexes are missing from the AQP complex. **c.** Detailed changes are conspicuous in the interactions between the KMSKS loop and the PPi mimic. Notably, a hydrogen bond between S194 and K192 in the ATP complexes is broken in the AQP complex, and both residues make strong hydrogen bonds to phosphate oxygen atoms.

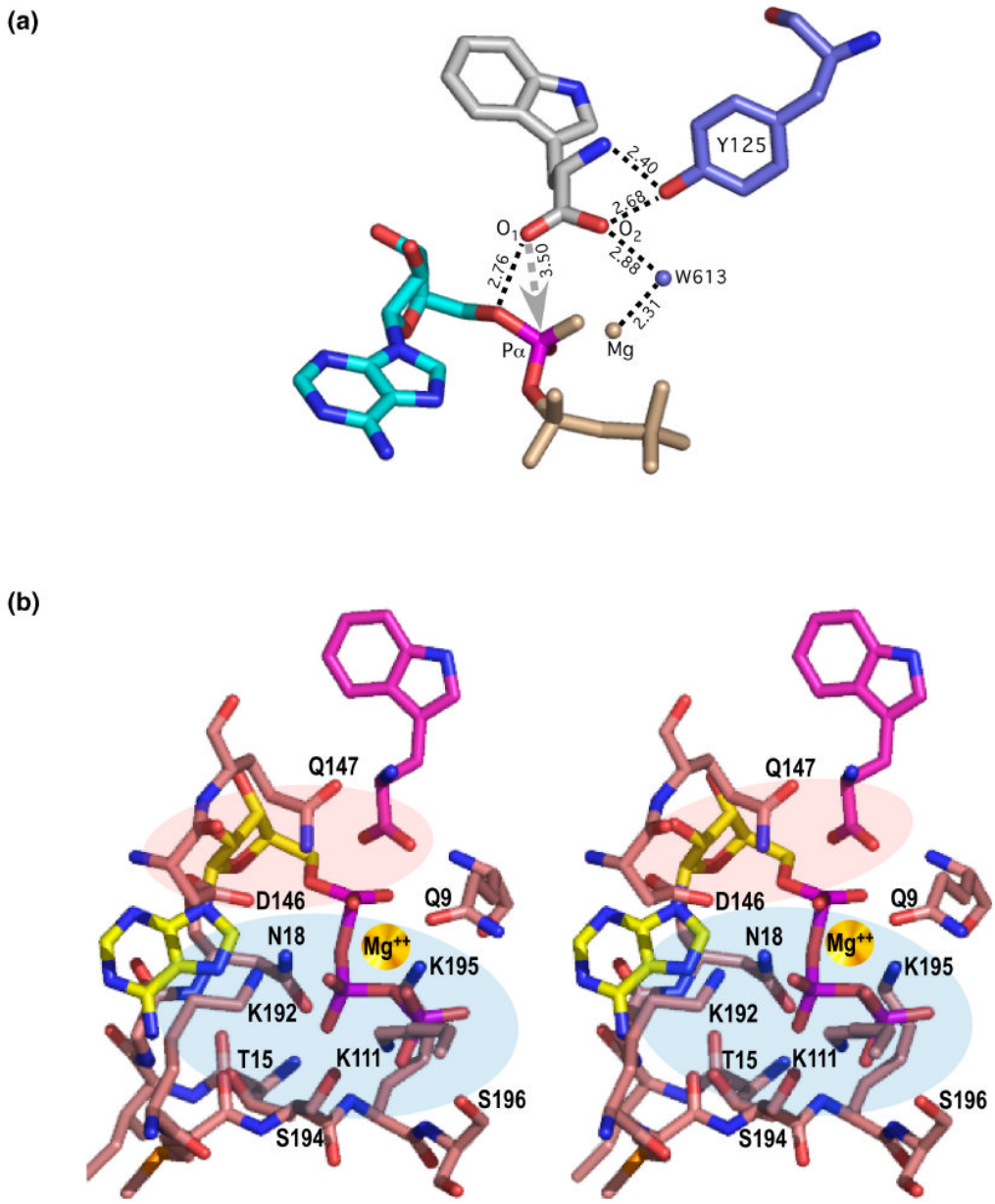

Figure 8.

Structure-based, schematic representation of the transition state for phosphoryl transfer by TrpRS. **a.** The environment of the carboxylate nucleophile. **b.** The active site showing the environment of the leaving pyrophosphate group. Light red and blue shaded ellipses indicate regions of negative and positive electrostatic potential arising from active site residues, and illustrated in Figure 9.

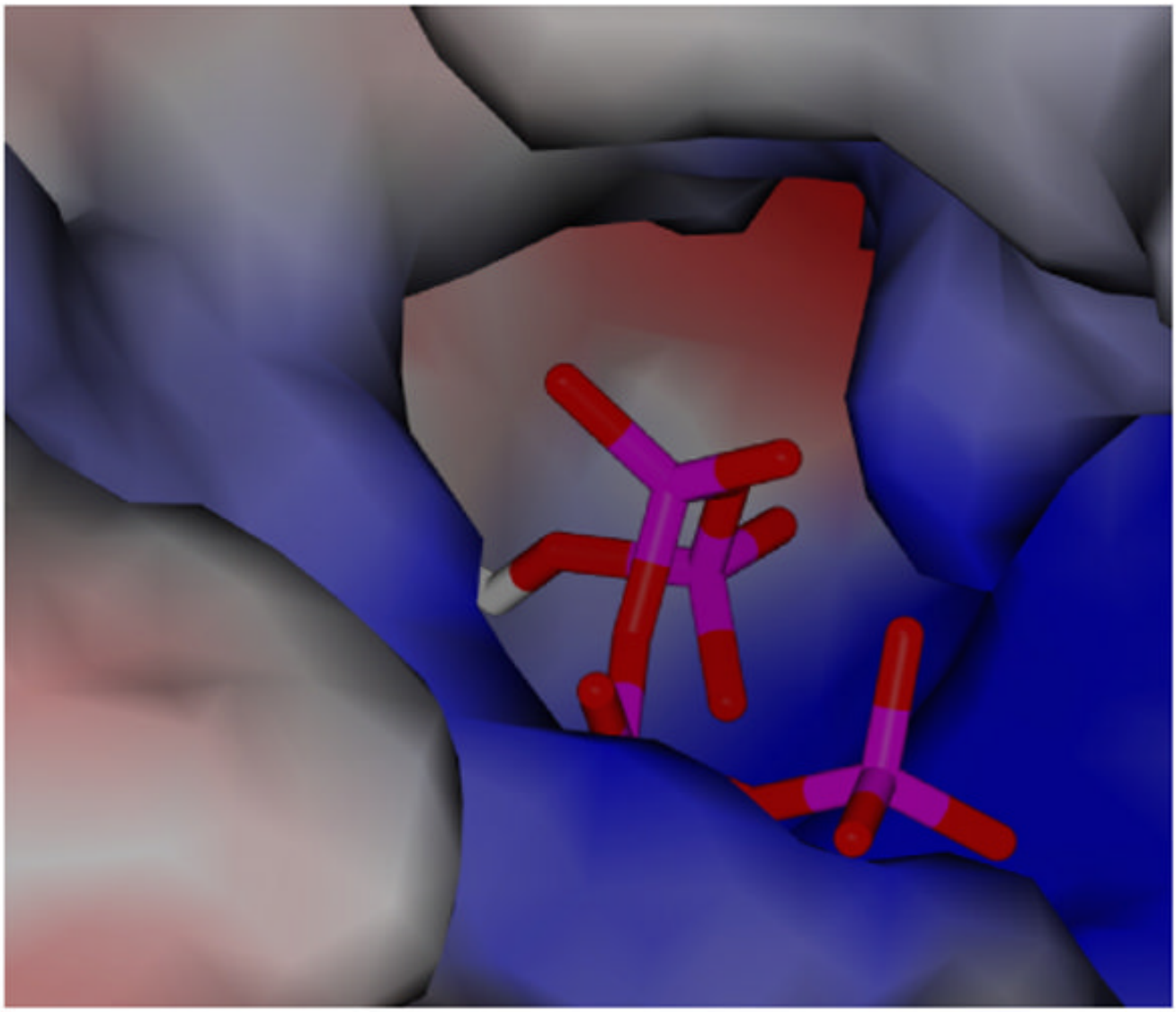

Figure 9.

Electrostatic surface charge density in the TrpRS active site. Red and blue colors represent positive and negative charge, respectively, on a range from −30 to 30 electron volts/Å^2. The ligand is AQP, and the γ- and δ- phosphate groups are nestled into the leaving group subsite, which is entirely surrounded by positive charge density. The α-phosphate and nucleophile are deep within the pocket and are surrounded by negative charge density (prepared with SPOCK).